Dissolution mechanism of cellulose in a benzyltriethylammonium/urea deep eutectic solvent (DES): DFT-quantum modeling, molecular dynamics and experimental investigation

Azougagh Omar, Jilal Issam, Jabir Loubna, El-Hammi Hayat, Essayeh Soumya, Mohammed Nor, Achalhi Nafea, El yousfi Ridouan, El Idrissi Abderrahmane, El Ouardi Youssef, Laatikainen Katri, Abou-Salama Mohamed, El Barkany Soufian

DOI: 10.1039/D3CP02335D

Dissolution Mechanism of Cellulose in Benzyltriethylammonium/Urea Deep Eutectic Solvent (DES): DFT-Quantum Modeling, Molecular Dynamics and Experimental Investigation

Omar Azougagh*[a], Issam Jilal[b], Loubna Jabir [a], Hayat El-Hammi [a], Soumya Essayeh[a], Nor Mohammed[c], Nafea Achalhi[d], Ridouan El yousfi[d], Abderrahmane El Idrissi[d], Youssef El Ouardi[b,e], Katri Laatikainen[e], Mohamed Abou-Salama[a], Soufian El Barkany*[a, c]

[a]*Laboratory of Molecular Chemistry, Materials and Environment (LMCME), Department of Chemistry, Faculty Multidisciplinary Nador, Mohammed 1st University, P. B. 300, Nador 62700, Morocco*
[b]*LIMOME Laboratory, Dhar El Mehraz Faculty of Sciences, Sidi Mohamed Ben Abdellah University, B.P. 1796 Atlas, Fes 30000, Morocco*
[c] *Applied Chemistry Unit, Sciences and Technologies Faculty, Abdelmalek Essaadi University, 32 003 Al Hoceima, Morocco*
[d]*Laboratory Applied Chemistry and Environmental (LCAE-URAC18), Faculty of Sciences of Oujda, Mohammed 1st University, 60000 Oujda, Morocco*
[e]*Laboratory of Separation Technology, Lappeenranta University of Technology, P.O. Box 20, FI-53851 Lappeenranta, Finland.*

**Corresponding authors. E-mail addresses: el.barkany011@gmail.com (Soufian El Barkany), o.azougagh91@gmail.com (Omar Azougagh)*

Abstract:

In this paper, the Benzyltriethylammonium/urea DES was investigated as a new green eco-friendly medium for the progress of organic chemical reactions, particularly the dissolution and the functionalization of cellulose. In this regard, the viscosity-average molecular weight of cellulose ($\overline{M}_w$) during the dissolution/regeneration process was investigated. It showed no significant degradation of the polymer chains. Moreover, X-ray diffraction patterns indicated that the cellulose dissolution process in BTEAB/Urea DES decreased the crystallinity index from 87% to 75%, and no effect was induced on type I cellulose polymorphism. However, the drastic impact of the cosolvent (water and DMSO) on the melting point of DES was inspected. Besides, to understand the evolution of cellulose-DES interactions, the formation mechanism of the system was studied in terms of H-bond density and Radial Distribution Function (RDF) using Molecular dynamics modeling. Furthermore, the Density Functional Theory (DFT) was investigated to evaluate the topological characteristics of the polymeric system (Potential Energy Density (PED)), Laplacian Electron Density (LED), energy density, and Kinetic Energy Density (KED)) at Bond Critical Points (BCP) between cellulose and DES. The Quantum Theory of Atoms in Molecules (AIM), Bader's Quantum Theory (BQT), and Reduced Density Gradient (RDG) scatter plots have been exploited to estimate and locate Non-Covalent Interactions (NCI). The results revealed that the dissolution process is attributed to the physical interactions, mainly the strong H-bond interactions.

Keywords: *Deep Eutectic Solvent (DES), Cellulose dissolution, Molecular dynamics (MD), Quantum Bader's theory, Benzyltriethylammonium/Urea, Density Functional Theory (DFT).*

1. Introduction:

Cellulose is the most abundant biopolymer on earth, and it offers excellent macromolecular and biological properties, particularly biodegradability, biocompatibility, and renewability [1]. In addition, this famous polymer constitutes the spine of the "green" industries, from the food industry to the pharmaceutical industry and building materials to green technologies and energy storage engineering.[2-4] However, because of its high melting point "degrades before melting, " [5] cellulose is excluded from formulations based on thermal processes, which constitute an essential part of industrial processes.[6] Therefore, chemical derivatization is the effective way to increase the economic and industrial values of this valuable renewable resource like fibers, films, food packaging, membranes, sponges, etc. [7-9] The homogenous functionalization of cellulose provides reasonable control of the polydispersity and the physicochemical properties of the polymeric systems, and this can only be achieved through a good understanding of the solubility phenomenon of cellulose, especially the supramolecular interactions. Cellulose dissolution is a highly complicated mechanism, where the hydrophobic and the hydrophilic areas are dispersed on the cellulose structure simultaneously,[10, 11] generated by the intra and intermolecular H-bonds orientations. These bonds result in strong supramolecular interactions, leading to the high stability of cellulose in most conventional solvents.[12, 13]

"Solvents" are chemical substances used to dissolve, extract, or suspend other compounds to form solution mixtures,[14] and are extensively used in industrial processes such as degreasing, cleaning, stripping, printing, painting, adhesives, pharmaceutical manufacturing, etc. [15]. However, traditional organic solvents are generally toxic and volatile (VOCs),[16] hence threatening environmental safety and public health.).[17, 18] In this sense, developing new eco-friendly and non-hazardous processes has become an imperative need, especially with the growing interest in green chemistry and sustainable industries.[19-21] Over the past decades, several alternative solvent categories to usual organic solvents have been developed and described as green, ecological, biodegradable, and sustainable,[22] and the majority of these families include supercritical fluids, ionic liquids, polarity-switching solvents, and deep eutectic solvents.[23-26] However, the Deep Eutectic Solvents (DES) have proven to be good candidates for the substitution of VOCs conventional solvents, as well as the elimination of the catalysts

requirement from reaction environments and treatment processes, and have attracted widespread attention due to their potential advantages, in particular, their catalytic effect which has recently been highly investigated as a new line of research.[27, 28] Moreover, the DES as low-melting solvent system is the seat of the physical combinations between the quaternary ammonium salts as H-Bond Acceptors (HBA) and other chemical species able to provide mobile protons and is considered as H-Bond Donor (HBD), where the counter-ion, often a halide, acts as an interactional bridge between the HBA and the HBD.[29, 30]

Since the first publication reported by *Abbott et al.* in 2003 investigating the solvent properties of choline chloride/urea mixtures,[31] The number of published scientific articles on the topic of DES applications has significantly increased,[32], therefore, the DESs become the first choice and the most popular solvent, especially for catalysis application,[32] biomass treatment, [33] biodiesel purification,[34] and electrochemical chemistry for their wide electrochemical window.[35] Therefore, DESs have emerged as the most promising reaction medium for valorizing natural resources and biomass dissolution without any additive.[36-38] Several DES systems have been reported and demonstrated appropriate ability for lignocellulosic material fractionation, cellulose dissolution and its chemical functionalization.[37, 39, 40] The effect of HBD on the dissolution efficiency of cellulose was investigated using CC-based DESs and imidazole (IM), urea, acetamide, ammonium thiocyanate, and caprolactam as HBD, where the CC/IM DES-system showed the highest cellulose dissolution capacity at around 2.5 wt.%. This result was attributed to the strong hydrogen bond basicity of Imidazole and dipolarity-polarizability interactions, therefore the addition of the Poly(Ethylene Glycol) (PEG) improved the cellulose dissolution capacity up to 4.5 wt.%, indicating that the cosolvent contributes significantly to achieve the energy equilibrium between DES and cellulose improving the dissolution efficiency.[41] Also, the synergic effect between the quaternary ammonium salt (HBA) and the HBD was demonstrated by comparing the dissolution capacity of microcrystalline cellulose (MCC) in choline acetate ChAc (HBA) and a different portion of tributyl-methylammonium chloride TBMACl (HBD), where the solubility was improved from 0.2 wt.% in pure ChCl to 6 wt.% in ChCl/TBMACl (8.5/1.5: w/w), respectively.[42] Furthermore, *Zhao et al.* yielded impressive results by replacing TBMACl with ethanolamine as HBD with ChCl, where the ChCl/ethanolamine based DES showed good extractability of cellulose from biomasses and high cellulose lignin removal capacities.[43] On the other hand, the DES can act as a solvent and reagent if the reaction

conditions are oriented in this regard. *Park et al.* revealed that the crosslinking reaction of cotton using benzophenone derivatives in CC/urea or CC/ethylene glycol (1:2) DESs, generated some reaction between DES and the crosslinking agent.[44] On the other hand, *Abbott et al.* established that the functionalization of cellulose and cellulose derivatives in DES exhibited excellent results, where CC/$ZnCl_2$ (1:2) DES showed exceptional efficiency as a medium reaction for cellulose O-acetylation,[45] and therefore as a catalyst for cellulose-based macro-initiator preparation.[46] The catalytic effect of DES, especially the HBD, was motioned by *Karachalios et al.* report, which described the application of CCC/urea (and imidazole) DES system for the cationization of pine-bark wood wastes. In this regard, the catalytic effect was attributed to the imidazole HBD, which provides a high cationic charge density to the resulting material. This material can then be used as an effective adsorbent for removing phosphates from aqueous environments.[46]

In this work, the cellulose dissolution capacity of Benzyltriethylammonium/urea DES was investigated. The effect of the cosolvent type on the Eutectic Melting Point (EMP) was studied. The results displayed a significant influence of polar protic cosolvent (H_2O) to decrease the EMP than that of aprotic polar cosolvent such as DMSO, where the liquid phase of DES was achieved at room temperature, from 60°C the EMP of pure DES,[47] by adding 2% of water and the same result was found by addition of around 10% of DMSO. The influence of the dissolution/regeneration process in BTEABr/urea (1:2) on the physicochemical properties of cellulose was investigated, and by succeeding the variation of the viscosity-average molecular weight ($\bar{M}_w$) between non-dissolved and regenerated cellulose, using the intrinsic viscosity measurements. Furthermore, the crystallinity index and the crystalline X-ray diffraction patterns studies showed a slight decrease in the crystallinity, but no effect was induced on the cellulosic polymorphism. In-depth theoretical studies complete the experimental results to understand the evolution of cellulose-DES interactions at the supramolecular level. The DES formation mechanism and its interaction with cellulose are investigated in terms of H-bond interaction density and radial distribution functions using molecular dynamics. The Functional Density Theory (DFT) quantum modeling the topological characteristics of the cellulose-DES matrix (potential energy density, electron density Laplacian, energy density, and kinetic energy density) are calculated at the Bond Crucial Points (BCP) using Atoms-In-Molecules (AIM) and Quantum Bader's theory. Furthermore, the Reduced Density Gradient (RDG) was exploited as a computational tool to determine the non-covalent interactions in the DES-cellulose system.

This paper is part of a global study that aims to design and find new green eco-friendly environment "solvents" for biomass valorization of natural resources and agricultural waste, especially the separation, extraction, dissolution, and functionalization of different biomass constituents (lignin, cellulose, and hemicellulose) and cellulose derivatives. In this regard, the development of new deep eutectic solvents as an eco-friendly medium constitutes the key stage of this project. However, even with the great efforts published recently,[48] the DESs formation mechanism and their behavior in the reaction medium remain poorly known.[49]

To our knowledge, the Benzyltriethylammonium/urea DES system was never discussed before in the literature as an eco-friendly solvent for cellulose dissolution and functionalization. Given the limited redaction area dedicated to scientific publication, this article is devoted to the quantification and distribution of competing interactions in the cellulose dissolution mechanism. In contrast, the following paper will be dedicated to the functionalization of cellulose and the catalytic effect of this new DES in organic chemistry.

2. Materials and methods

Materials

Cellulose powder (M_w ~35.5 10^3 Da) was purchased from Sigma Aldrich Company. Triethylamine (TEA), benzyl bromide, and urea were obtained from Fluka. Tetrahydrofuran (THF), diethyl ether, acetone, and other solvents were received from Merck. All chemicals and solvents are analytical grade and were used as received without any further purification.

Instrumental analysis

The crystalline patterns of non-dissolved and regenerated cellulose (regn-Cell) samples were recorded on X-ray Diffractometer *EQUINOX 2000* using CuKα (λ=1.5418A°) radiation at 40 kV and 30 mA as accelerating voltage and operating current, respectively. All patterns were registered in the range of 2θ (0°– 40°). The average molecular weight values of non-dissolved and regenerated cellulosic samples were estimated using the Mark-Houwink equation $[\eta] = KM_w^a$ where k and a are the constants describing the specificity of the polymer-solvent pair depending on the temperature. Therefore, the intrinsic viscosity $[\eta]$ was derived from the linear dependence and the extrapolation of the reduced (η_{red}) and the inherent viscosity (η_{inh}) to zero concentration. In this regard, the different viscosities were measured from the flow time of the

polymeric solution through the Ubbelohde viscometer glass capillary at 25 °C in NaOH/Urea/H_2O solvent.[50]

Preparation of DES and cellulose dissolution:

BTEABr/urea DES was prepared according to the method reported by *Azougagh et al.* in our previous paper.[51] In short, 4.5 ml (38 mmol) of benzyl bromide was reacted with an equimolar amount of TEA (5 ml, 36 mmol) in THF as solvent at room temperature. The white crystal (BTEAB salt) was recovered by vacuum filtration, frequently washed with diethyl ether, and dried in a vacuum desiccator to constant weight. The DES (BTEAB/Urea, 1/2) was carried out by mixing 3 g of BTEAB salt (11 mmol) and 1.5 g of urea (25 mmol), where the reaction mixture becomes liquid under stirring in the range of the temperatures around 60 °C. The effect of cosolvent on the Eutectic Melting Point (EMP) was investigated, given ratios of water and DMSO as polar protic and polar aprotic cosolvents, respectively. The cellulose dissolution capacity of BTEAB/urea DES was studied at concentrations ranging between 2 % and 11 %, where the DES was heated at T_{EMP} + 20 °C for 30 min to ensure the thermodynamic equilibrium between HBA and HBD. Then, the temperature was decreased to 60 - 70 °C, a given amount of cellulose was added to DES, and the mixture was stirred under reflux for 1 hour. The regenerated cellulose was recovered by precipitation in water, filtered under reduced pressure, washed with water and acetone, and kept in a P_2O_5 desiccator for one week.

Theoretical background

DFT-Quantum calculations

Polysaccharides generally show a remarkable water-affinity against pH, especially starches (native or modified) which have demonstrated a significant increase in swelling power and solubility in alkaline regions between pH 8 and 12.[52] On the other hand, the protonic behavior of chitosan allows it to be considered as a weak base soluble in aqueous solutions of weak acids (pH<6.5) e.g. acetic acid.[53] However, cellulose constitutes a structural exception of carbohydrates, where the strong crystallinity and the high density of H-bonds generate a structural poly-biphasic anisotropy (hydrophilic and hydrophobic regions),[54, 55] which complicates our understanding of cellulose dissolution mechanisms. This anisotropy makes cellulose insoluble in common solvents due to the prevention and limitation of reaching equilibrium between competing forces during cellulose dissolution, including hydrogen

bonds.[56] Recently, DESs have shown a high ability to disrupt the structural stability of cellulose, which indicates their aptitude to disturb and interrupt the intra and intermolecular H-bond network of cellulosic fibers [40]. However, the cellulose dissolution mechanisms in DESs are still incompletely elucidated, and several mechanisms are proposed using numerous computational and modeling calculations.[57] In this work, the cellulose dissolution capacity of the new BTEAB/Urea DES was investigated using DFT, which gives the distribution and the quantification of the competing interactions during the dissolution process, at the supramolecular level. In this concern, the estimation of the H-bonding electronic properties and its chemical environment was turned using the cellulose dimer as a calculation model to simplify the computational calculations. In addition, Becke's three-parameter hybrid exchange functional (B3),[58] the LYP correlation functional,[59] and the 6-311+G (d,p) basis set at the density functional approach has been used to calculate molecular geometries and their electronic wave functions in current systems. In molecular simulation, the gas phase molecular structures of cellulose dimer, DES, and cellulose-DES complex were constructed. The chemical configurations of the cellulose dimer, DES, and the cellulose-DES complex were verified to be local minima by frequency calculations, and imaginary frequencies absence, ensuring minimum attendance. The Gaussian 09 suite of software tools[60] was first used, in this work, to optimize the configurations and then to calculate the vibrational frequencies. Furthermore, the Electrostatic Potential Surfaces (EPS) were generated and plotted for each molecule via the Gauss-View 05 software.[61] The strength and the nature of the intermolecular interactions were then studied extensively using the Atom In Molecules (AIM) analysis at the Bond Critical Point (BCP)[62] and the Reduced Density Gradient (RDG) analysis[63] based on the optimized geometry at B3LYP/6-311+G(d,p) level. The results were obtained using the Multiwfn program code ,[64] and the mapped 3D iso-surface plot that was produced with the VMD software packages.[65]

Topological Analysis

Bader describes binding paths, corresponding to the trajectories connecting two attractors and passing through a critical point called the Critical Binding Point (BCP).[62] This point corresponds to the minimum local electron density along the bond path and the maximum along the perpendicular plane and is directly related to the topological AIM analysis calculations. According to Bader's theory, the presence of a "bond path" or a BCP between two atoms is the necessary and sufficient condition for the existence of a chemical bond between the two atoms

involved.[66] Well, the total electron density (ρ(r)) and its related Laplacian ($\nabla^2\rho(r)$) indicate the nature of the bonds, where the total Laplacian electron density is given by the following formula (Eq. 1). V(r) and G(r) are potential energy densities and Lagrangian kinetic energy at critical points, respectively.

$$\frac{1}{4}\nabla^2\rho(r) = 2G(r) + V(r) \qquad (Eq.\ 1)$$

The relationship between the kinetic energy density G(r) and the potential energy density V(r) provides important information about the depletion or concentration of electron density,[67] and therefore the nature of the bond, where values of G(r) > 0 while V(r) < 0 are always validated at critical points.

Viriel's theorem, applied to BCP, implies that interactions with negative ∇2ρ (r) mean an excess of potential energy V(r) at BCP. This type of interaction is electron-shared interaction and usually occurs between atoms connected by a "covalent bond".[68] Inversely, the interactions with positive values of the Laplacian (∇2ρ(r) > 0) are dominated by local excess of kinetic energy, where the contribution of kinetic energy G(r) is more significant than that of potential energy V(r), and they are closed shell interaction which generally corresponds to non-covalent interactions.[69] Alternatively, Cremer and Krak have proposed a different approach to evaluating the strength and nature of interaction at the BCP.[70] This method combines the Laplacian of the electron density ∇2ρ(r) along with the total electron energy H (r). The electronic energy density H(r) at BCP is given by Equation 2:

$$H(r) = G(r) + V(r) \qquad (Eq.\ 2)$$

Reduced Density Gradient (RDG):

Topological methods often attempt to study regions with high electron density in order to rationalize the interacting molecular structures. However, the weak or non-covalent interactions of regions with low electron density have been successfully described by the RDG, which is a dimensionless fundamental quantity in the recently developed DFT, also known as the Non-Covalent Interaction (NCI) method.[63, 71] The RDG, as a function of density ρ and its gradient |∇ρ| (Eq.3), allows the identification and the visualization of weak interaction zones as well as

the qualitative access to the strength of these non-covalent interactions involved in the structure of the studied system.

$$RDG(\rho) = \frac{1}{(2\pi^2)^{1/3}} \frac{|\nabla\rho|}{\rho^{4/3}} \qquad (Eq.\ 3)$$

The RDG is a dimensionless fundamental quantity used to represent the deviation from a homogeneous distribution of electrons, which can be counted at any point in space (and especially at any point in a 3D-grid of space).[72] In the regions located very far from the molecule, where the density ρ decreases to zero exponentially, the reduced gradient will have very large positive values towards infinity (since its term in ρ-4/3 dominates its behavior). However, the reduced gradient gets lower values, near zero, in the regions of covalent and non-covalent interactions. Since the DGR (ρ) behavior is governed by |∇ρ|, non-covalent interactions can be identified as low density and low gradient areas.[73] The density values of the low-gradient zones appear to be an indicator of the interaction strength as well. However, very different types of interactions emerge in the same region of density/reduced gradient space.[72] Consequently, it is impossible to identify the interaction nature and, in particular, to distinguish between stabilizing and repulsive interactions (VDW interaction, repulsion, H-bonding...). So, to get an insight into the nature of the interaction and to understand bonding in more detail, it is possible to analyze the sign of the second eigenvalue (λ_2) of the Laplacian density (Eq. 4):

$$\nabla^2\rho = \lambda_1 + \lambda_2 + \lambda_3 \qquad (Eq.\ 4)$$

When the local repulsion is balanced by inter- or intra-molecular attractions, the effect is stabilized and non-covalent bonding develops between the involved fractions. This situation corresponds to the most typical case of hydrogen bonding, which occurs between a donor and an acceptor, where such interactions correspond to the values of $\rho > 0.01$ u.a and $\lambda 2 < 0$. Moreover, the electron density value ρ at the tips is proportionally dependent on the strength of the interactions.[74] But, when local repulsion is not balanced by significant local attractions, the stable geometry results from interactions between pairs of atoms as external constraints, which refer to the state where the repulsion arises from neighboring atom contributions. However, this situation is associated with the positive value of λ2 that corresponds to the steric repulsion, where such interactions are associated with the values of $\rho > 0.01$ u.a. and $\lambda 2 > 0$.[75] Between

these two limit cases, the critical points that occur at very low density values were considered as the third weaker interaction type. In these regions, the density and gradient are both low (usually < 0.01 u.a), and so λ2 is near 0. In fact, this situation is most common for attractive and weak interactions such as the VDW forces.[76] Therefore, we can define a real sign(λ_2)ρ space function, i. e. the product of sign of the second largest Eigenvalues of the Hessian matrix λ_2 and ρ.The *sign*(λ_2)ρ can then be mapped to RDG isosurfaces using the color bar below,[77] which reveals where weak interactions occur and intuitively catches the interaction genre.

Molecular Dynamics Simulation Details

MD simulations for all the structures analysed were conducted with the DESMOND software[78]. Forcefield parameterizations for all materials considered (DES, cellulose:DES) is OPLS 2005 . The structures considered for this work were:

- Periodic DES system (i.e. DES containing 120 BN cations + 120 Br^- anions + 240 URE, equivalent to the equimolar mixture of BN^+: Br^-:Urea all at a 1:1:2 mol ratio).
- Periodic cellulose:DES system (i.e. cellulose: DES containing 3 crystallin cellulose oligomers (DP=8) + 120 BN^+ cations + 120 Br^- anions + 240 UREA, equivalent to the equimolar mixture of cellulose monomer:DES all at a 1:5 mol ratio).

MD simulations have been conducted as an NPT ensemble giving the experimental conditions. Temperature and pressure were controlled using the Nose-Hoover method, with all simulations performed at 348 K (except for Periodic DES system simulations performed at 308, 318, 328, 338, 348, 358 and 368 K) and at 1 bar. The motion equations were integrated using the RESPA integrator method with a time phase of 2 fs. Lennard-Jones encounters were handled with possible 15 Å cut-offs and Periodic boundary conditions have been applied in all directions. 20 ns long MD Simulations have been used for all the studied systems.

3. Results and discussion:

3.1. DFT-Quantum Modeling:

*Electrostatic Potential surface (*EPS)

The Electrostatic Potential Surface (EPS) map is a useful descriptor for defining the total charge 3D distribution, molecular size, and shape of the molecules in terms of color coding (colored against the distribution of electron density on the molecular surface),[79] which is very

beneficial to find the most probable binding receptor site in the molecule (electrophilic and nucleophilic sites). Therefore, EPS provides a visual representation of the chemically active sites by generating the electrostatic potential around the molecular geometry.[80] Conventionally, the red color indicates regions of electron-rich or partially negative charge indicating the site of the electrophilic attack, while the blue color indicates electron-deficient regions or partially positive charge making the site favorable for nucleophilic attack.

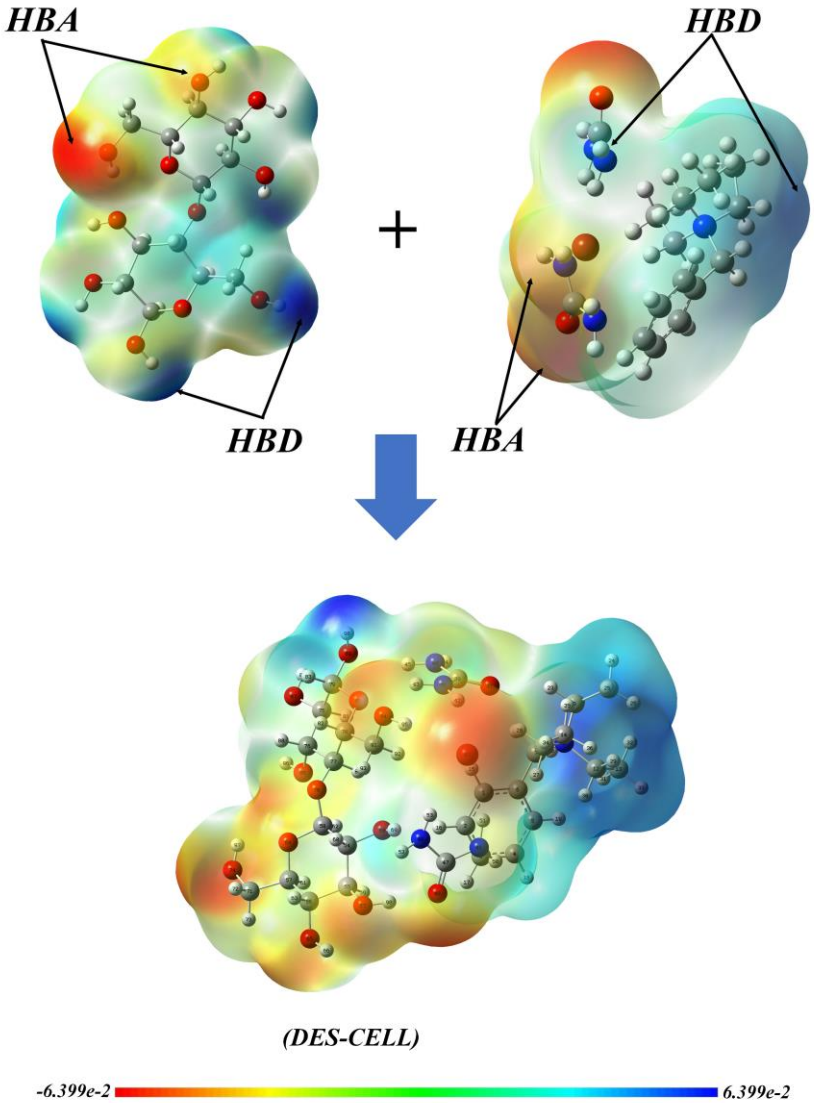

Fig. 1: Optimized configurations and EPS (Isovalue 0.005) mapped on electron total density of Cellulose dimer, DES, and DES-CELL system

To better understand the interaction mechanism between cellulose and the BTEAB/Urea DES, the distribution of electrostatic potentials at isosurfaces 0.005 were investigated, and the

cellulose, DES, and cellulose-DES system EPS maps are shown in Fig. 1, where the location of the positive and negative potentials is displayed using the blue and the red colors, respectively. The DES EPS map exhibited the positive electron-depleted regions (blue) around the quaternary nitrogen atom of BTEAB (HBA), near the H-urea (HBD) and benzyl rings.[51, 81] In addition, the most negative regions are observed closer to the Bromide ion and the carbonyl oxygen atom of urea. The cellulose dimers EPS showed that the most positive potential values were detected on the proton hydroxide, where the oxygen atoms constitute the colonies of the most negative potentials (Fig. 1).

During the cellulose dissolution process in DES, the positive (or negative) regions can interact with any negative (or positive) site of the DES solvent, thus generating a directional interaction. Therefore, the lowest electrostatic potential values of the electron-enriched regions of DES, located explicitly around the urea oxygen and the bromine atom, represent the most electrophilic sites to be considered as hydrogen bond acceptors and electrostatic interactions.[82] On the other hand, the hydrogen hydroxide of the cellulose offered the highest potential values zones characterized by low electron density and established a nucleophilic character to be the most probable area of H-bonding and electrostatic interactions. In addition, the interaction between the oxygen hydroxide of cellulose (the most cellulosic nucleophilic area) and the H-urea (the most electrophilic zones of DES) is strongly suggested. Moreover, the solvent environment itself can influence the electrostatic potential distribution within cellulose. Solvents with more and higher positive (or negative) regions can enhance the solvation of cellulose, leading to a redistribution of charges and alterations in the electrostatic potential landscape. This, in turn, affects the interactions between cellulose and solvent molecules, ultimately influencing the dissolution behavior. In this field, *Zhihan Tong et al* reported previously that the negative electrostatic potential (high electron density) areas in the metal salt hydrate based DES are preferentially combined with the positive electrostatic potential (low electron density) regions of cellulose.[83] This supports the notion that electrostatic interactions play a significant role in the dissolution process. Furthermore, similar conclusions have been reported before by *Hui Fu et al* investigating the dissolution behavior of microcrystalline cellulose (MCC) in DBU-based DESs [57].

Topological Analysis:

Through the topological properties of electron density and its derivatives related to the Critical Points of CPs and bonding paths, Bader's theory of atoms in molecules provides important details on the nature and classification of binding interactions.[84] Also, the combination of the interatomic distance, as a geometric parameter, with the corresponding topological properties proves to be an excellent method for accurately identifying the nature and strength of chemical bonds.[85] In the case of this study, the most significant BCPs of NCI in the DES-CELL system were obtained from the AIM approach and are illustrated in Fig. 2. The QTAIM analysis revealed the presence of two categories of BCPs: intermolecular BCPs between cellulose dimers and DES, and intramolecular BCPs in DES between the two components of DES (HBD and HBA). The AIM Image revealed the formation of three BCPs (BCP123, BCP128, and BCP197) as intramolecular BCPs between BTEAB and urea, and that in the linear reaction paths of H-urea (53) ⋯Br (37) H-urea (51) ⋯Br (37) H-urea (42) ⋯Br (37), where the interatomic distances H⋯Br were 2.67, 2.52 and 2.69 Å, respectively.[86] These results are consistent with the recent findings reported by Chai et al. in their recent publication, which focused on the structural analysis of Choline chloride $(ChCl)^-$carboxylic acid deep eutectic solvents (DESs). In their study, Chai et al. identified strong hydrogen bonding interactions between Cl^- and AA/FA, as well as between the carbonyl oxygen in AA/FA and the hydroxyl group of Ch^+. Furthermore, weak hydrogen bonds were observed between the methyl groups of ChCl and the carbonyl oxygen in AA/FA, with bond lengths ranging from 2.64 to 2.77 Å and 2.50 to 2.60 Å. The consistency between these research findings provides further support for our existing understanding of hydrogen bonding interactions in DESs.[86] However, the interaction between cellulose and DES gives rise to many different BCPs (BCP100, BCP105, BCP122, BCP144, BCP181, BCP233, and BCP247) in the reaction paths of $H_{cell}(98)\cdots O_{urea}(49)$, $O_{cell}(67)\cdots H_{urea}(52)$, $H_{cell}(62\cdots N_{urea}(48)$, $H_{cell}(67)\cdots Br(37)$, $H_{cell}(95)\cdots Br(37)$, $O_{cell}(85)\cdots H_{urea}(43)$, $O_{cell}(89)\cdots H_{urea}(45)$, where the distances of the intermolecular interaction paths are all within the range of 1.89 to 4.12 Å (Table SD1). It is interesting to note that the non-bonded (non-covalent) interactions in the DES-CELL system were identified as H-bonds, and that is due to the short distance between atoms,[87] which are long compared to the length of the covalent bond and shorter than the sum of the VDW distances,[88] except the BCP105 ($O_{cell}(67)$---H_{urea} (52)) and BCP144 (H_{cell} (67)---Br (37)) which are regarded as electrostatic or van der Waals interactions (4.12 Å).[89]

Along with the interatomic distance, the nature of chemical bonds between atoms and molecular reactivity can be described by the values of the topological parameters at BCP.[90] Physical quantities such as the total electron density ρ(r), Laplacian electron density $\nabla^2\rho(r)$, and electron energy density H(r) (proportional to the electron potential energy density V(r)) have great significance in the classification of the bonding interactions taking place in the molecular system.[91] The values of the DES-CELL AIM topological parameters (Table SD1) indicate that the balance between the electron energy density H(r) and the Laplacian total electron density ($\nabla^2\rho(r)$ gives a rich and straightforward understanding of the nature of the interatomic interaction established between the two atoms involved.

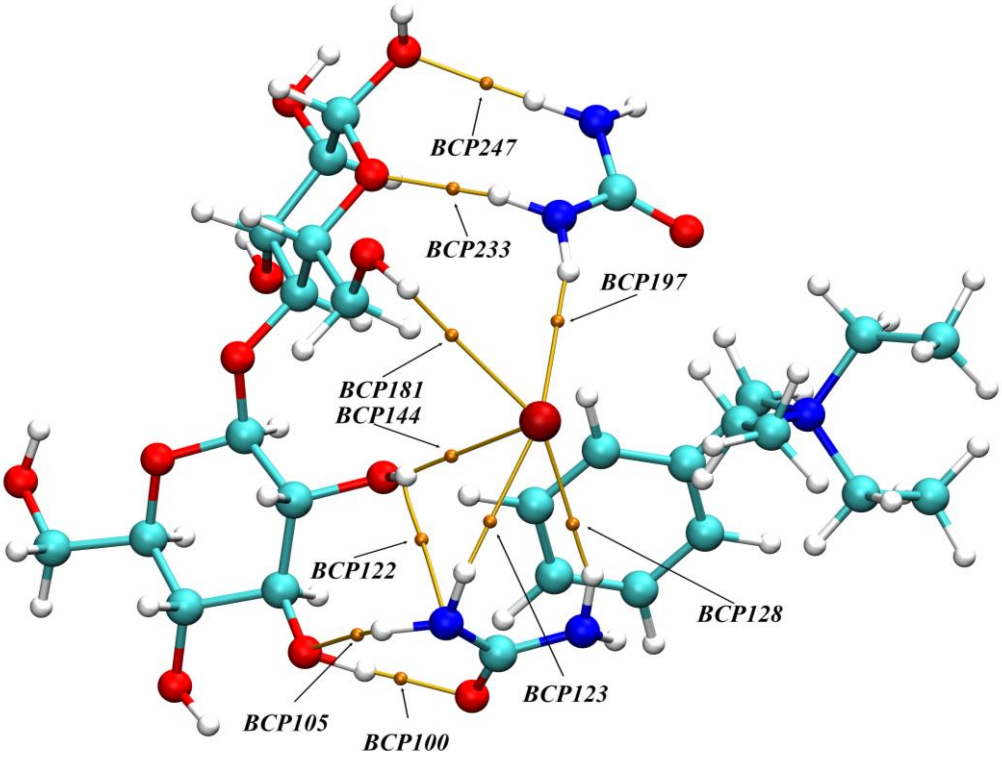

Fig. 2: Topological atoms in molecules (AIM) graph of the DES-CELL system

Indeed, according to the sign of ($\nabla^2\rho(r)$ and H(r), the interaction strength has been classified into three categories: *i)* $\nabla^2\rho(r) < 0$ and $H(r) < 0$ at the BCP indicates that the molecules interact strongly, known as "*shared-shell interaction*", and also defined as an electron-rich zone that can be attributed to free pairs of electrons as well as to covalent chemical bonds,[92] *ii)* $\nabla^2\rho(r) >$

0 and H(r) < 0 reflects that the system is governed by moderate interactions (H-bonding interaction) and *iii)* $\nabla^2\rho(r) > 0$ and H(r) > 0 reveals weak interactions (electrostatic interaction or weak H-bonds).[66] Unlike the first category, the last two are defined as "*closed-shell interactions*" between the two atoms and indicate an electron deficiency at the BCPs. Table SD1 shows the computed topological BCP parameters of DES-CEL. The positive values of $\nabla^2\rho(r)$ range from 0.033 to 0.034 a.u., and the positive H(r) values diverge from 0.0012 to 0.0014 a.u., indicating that the electrostatic or weak H-bonds interactions occurred between BTEAB and two urea molecules.[93] However, the positive values of all $\nabla^2\rho(r)$, which range from 0.012 to 0.12 a.u. between cellulose and BTEAB-based DES indicate the non-covalent interaction nature. In addition, the strength of the H-bond can be classified according to the sign of H(r), where H(r) < indicates a strong or medium H-bond, while H(r) > 0 suggests weak hydrogen bond interaction.[94] Given the results in table SD1, the negative value of H(r) (H(r) = -0.0015 a.u) of $H_{cell}(98)\cdots O_{urea}$ (49) at BCP100 is a strong indication of the interaction between cellulose and DES by strong or moderate H-bonding interactions. In contrast, the positive H(r) values ranging from 0.00046 to 0.00235 at BCP105, BCP122, BCP144, BCP181, BCP233, and BCP247 assume that the interactions, between DES and cellulose are H-bonding (*closed-shell interactions*) that dominated by weak H-bonds interaction.[95, 96]

Additionally, bond strength can be measured by the magnitude of ρ(r), where the strongest bond is associated with the largest ρ(r) value. The data listed in Table SD1 shows that the *ρ(r)* values within the range of 0.006 to 0.04.u.a of BCPs between DES and cellulose in the DES-CELL system are more significant than that for intra BCPs in DES. Among the H-bond interactions in the DES-CELL complex, the Hcell(98)···Ourea(49) bond exhibited the strongest strength, characterized by a ρ(r)= 0.039 a.u. Importantly, these values are generally higher than those previously reported in the literature and recommended by Koch and Popelier (0.002–0.0274 a.u)[97], highlighting the significant bonding characteristics observed in this study. Li et al. have reported ρ values ranging from 0.002 to 0.035 a.u in the dissolution of cellulose using a combination of metal chlorides (ZnCl2, LiCl, or NaCl) mixed with AmimCl ionic liquid.[98] which shows that the cellulose will be more favorable to combine easily with BTEAB/urea.[99] indicating that the BTEAB/Urea is strongly suggested as a reaction medium to the cellulose dissolution and functionalization. Therefore, this result confirms that the urea-based DES appears to be the most effective solvent, which can dissolve cellulose through HBs between urea molecules and the released –OH groups on cellulose chains, resulting in severe swelling

of cellulose fibers in DES and subsequent dissolution. Furthermore, the results obtained in this paper are in good agreement with previous studies investigating the insightful role of urea in cellulose dissolution. [100-102]

Reduced Density Gradient (RDG):

Within the AIM theory, the RDG approach provides a valuable tool to distinguish between different types of weak interactions, which allows graphical visualization of the distribution of non-covalent interaction regions in real space.[103] According to the RDG scatter plots as a function of the sign (λ2) ρ(r) and RDG isosurfaces (Fig. 3), the RDG method was successfully applied to distinguish the strength and the type of multiple non-covalent interactions in the DES-CELL matrix using the color-mapped isosurfaces, where the surfaces are colored on a blue-green-red scale according to values of sign (λ2)ρ, and that is from ~~a~~ strong attractive interactions such as H-bonds (blue color) to higher repulsion (red regions), whereas the green regions indicate the electrostatic interactions.[104, 105]

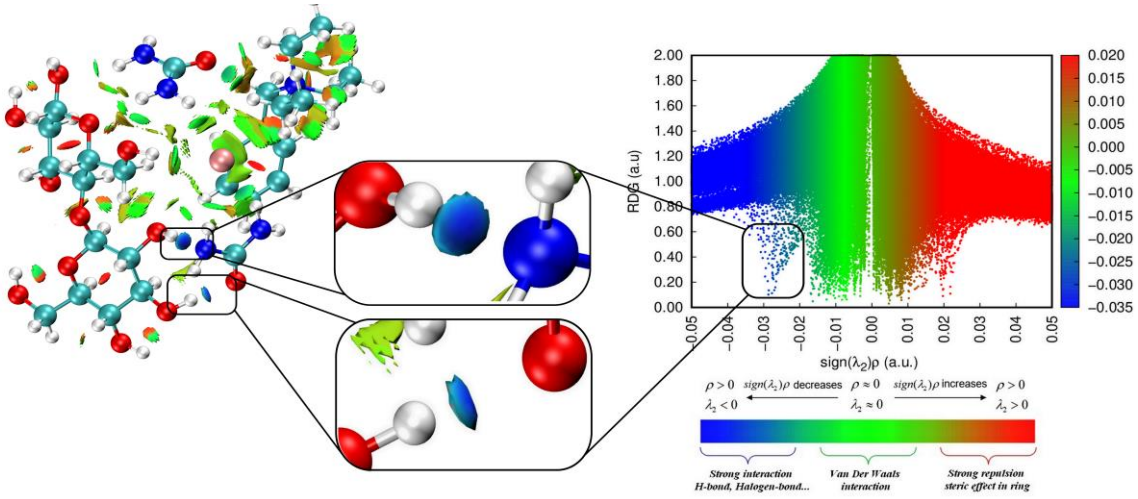

Fig. 3: RDG against sign (λ_2)ρ isosurface scatter plot and RDG analysis of the DES-CELL

The reduced density gradient function scatter plot versus the sign(λ_2)ρ ranging from -0.05 to +0.05 a.u of cellulose-DES complex (Fig. 3) displayed the presence of highly reduced density gradient spikes at negative density values of sign(λ_2)ρ ($\rho < 0.05$), which indicates the existence of non-covalent interactions.[103] Moreover, the nature and strength of these interactions can be distinguished depending on the location of the spikes, where the coexistence of strong-attractive dispersion interactions between cellulose and DES are indicated by the presence of the spike at

sign ($\lambda 2)\rho$ < -0.03 a.u. It can be compared to spike at -0.036 a.u, [106] reported by Zhang et al. for the interaction of lignin with imidazolium-based ionic liquids. On the other hand, the spike at a positive sign ($\lambda 2)\rho$ value (0.02 a.u.) is attributed to the steric effect.[107] However, the large spike at sign(λ_2)ρ values of -0.02 to 0 a.u indicates the presence of weakly-attractive dispersion interactions.[108] Furthermore, RDG isosurfaces (3D-plot) were explored to visualize the spatial location of chemical interactions in the complex formed by cellulose and BTEAB/urea EDS (Fig. 3). Therefore, the different types of color-filled RDG isosurface regions were distinguished by analyzing the surface color shift (red-green-blue scale) given the sign(λ_2)ρ.[51] The sign ($\lambda 2)\rho$ negative values (blue color) indicate the strong attractive interaction between cellulose and DES, in particular between Ocell(67)•••Hurea (52) and Hcell(98)•••Ourea (49) that display blue-light color of the disc-shaped slab, indicating the occurrence of strong H-bonding interactions. In addition, the $H_{cell}(62)\cdots N_{urea}$ (48), H_{cell} (67) ⋯Br (37), $H_{cell}(95)\cdots$Br (37), $O_{cell}(85)\cdots H_{urea}$ (43), and $O_{cell}(89)\cdots H_{urea}$ (45) bond interactions are clearly exhibited by elliptic RDG isosurfaces with green-blue color in the central regions of contact, which reveals the existence of weak H-bonds and electrostatic interactions between the different sites. However, the electrostatic interactions were strongly suggested between the constituent entities of DES (green color), where the strong "red" steric interaction regions were detected at the benzene center and glucose ring. These results are in good agreement with the previously published theoretical studies on the cellulose interactions mechanism with DES and ILs.[57, 83, 95] According to the RDG results, the mechanism of cellulose dissolution in BTEAB/urea DES involves the different types of NCIs, including strong and weak H-bonds and electrostatic interactions, which can coexist at such contribution. In addition, agreeing to AIM calculations and geometric and topological analysis, the progression of cellulose dissolution is strongly dominated by strong H-bond interactions, where the results showed that the region and the force of attraction between cellulose and HBD are considerably stronger than those between cellulose and HBA, suggesting a primordial role and an important contribution of urea to the cellulose dissolution process.

Our results agree with the research conducted by *Zhang et al*., who investigated the interactions between ionic liquids (ILs) and a model lignin compound. In their study, they utilized various theoretical methodologies, such as DFT, AIM, NBO, and RDG, to explore the dissolution mechanism of lignin in imidazolium-based ILs. The computational data provided insights into the dissolution mechanism. They emphasized the significant role of hydrogen bonding (H-

bonding) in facilitating the dissolution of lignin in ILs, which is consistent with experimental evidence. [106]

Cao et al.[95] also examined the mechanism of cellulose dissolution in acetate-based ILs using cellobiose and BmimAc as a model system. Their findings revealed that hydrogen bonds and van der Waals interactions between cellobiose and ILs play pivotal roles in the dissolution process. Electrostatic Potential analysis was employed to identify reactive sites on the molecular surface, aiding in determining the most stable configuration. The geometrical analysis provided insights into the complex formed by cellobiose and [Bmim]OAc. The study utilized AIM theory to examine the characteristics and variations of bond types at Bond Critical Points (BCPs). Noncovalent interactions within the complex were comprehensively characterized and visualized using RDG analysis.

3.2. Molecular Dynamics (MD):

The molecular structure of BTEAB/urea DES (benzyl triéthyle ammonium (N^+): Bromide ion (Br^-): Urea) was investigated in terms of H-bond densities and radial distribution functions. The MD simulation analysis of DES (Fig. 4) showed that the H-bond interaction densities given temperature had enfeebled brusquely and continuously above the Eutectic Melting Point (EMP), this behavior indicates the strong destruction of physical interactions, especially H-bonds, which the phase-change transformation is strongly suggested, and therefore the MD results are in good agreement with the experimental effects and confirming the DFT results obtained previously. However, the salt bridge (between N^+ and Br^-), the Pi-Pi stacking (between benzyl groups), and the Pi-cation (between N^+ and benzyl groups) interactions are slightly or not sensitive to temperature changes.[109] Moreover, the results show that the constituents of EDS (N^+, Br^-, and urea) are not amphiphilically structured, and this is due to remnants of Pi-Cation interactions. Thus, the polar domain consists of a variety of H-bonds and electrostatic (salt bridge, pi cation) interactions (i.e. cation-bromide, cation-urea, bromide-urea, and urea-urea), whereas in the nonpolar domain, solvobic segregation is strong for Benzyltriethylammonium which leads to benzylic clusters.

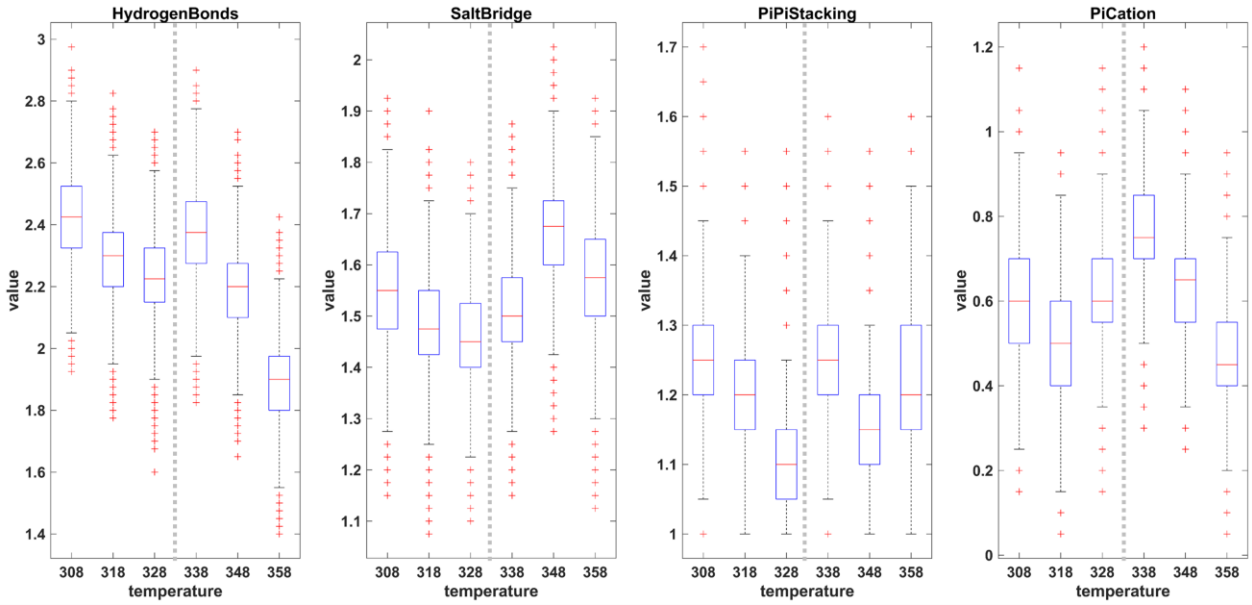

Fig. 4: Intermolecular interaction densities in DES at 308-358 K, the line at 323K indicate the Eutectic Melting Point (EMP)

To study further the nature of interactions between these components, Radial Distribution Functions (RDFs) study was implemented. The behavior of BN^{+}: Br^{-}: Urea DES was initially evaluated for 308 - 368 K and 1 bar using RDF center-of-mass radial distribution functions as reported in Fig. 5. Fig. 5a shows the organization of bromide within the polar DES network. The RDFs for the bromide around urea oxygen, ammonium, and urea nitrogen have clear peaks at 5.4 Å, 4.8 Å, and 3.7 Å respectively, indicating strong H-bonding between Br^{-} and hydrogen urea, resulting in the competition between ammonium and amino urea on binding with the bromide.[110] On the other hand, the organization of ammonium within the polar DES network is shown in Fig. 5b. The RDFs for the ammonium around urea nitrogen, urea oxygen, and bromide ion have maximum peaks at 5.5 Å, 4.5 Å, and 4.8 Å respectively, resulting in a competition between bromide and urea for binding sites with the cationic ammonium group.[111] It should be mentioned that the RDFs of cationic ammonium groups and bromides are slightly sensitive to temperature changes, especially for N(urea) and O(urea), where the peaks decrease at temperatures above the EMP, which explains the decrease in H-bond densities (Fig. 4). The RDF results confirm the DFT calculations indicating a weakening of interactions between N^{+} and N^{+} ions and interactions within urea molecules in the DES. Moreover, RDFs revealed more interactions between Br^{-} ion and the amino group of urea components.

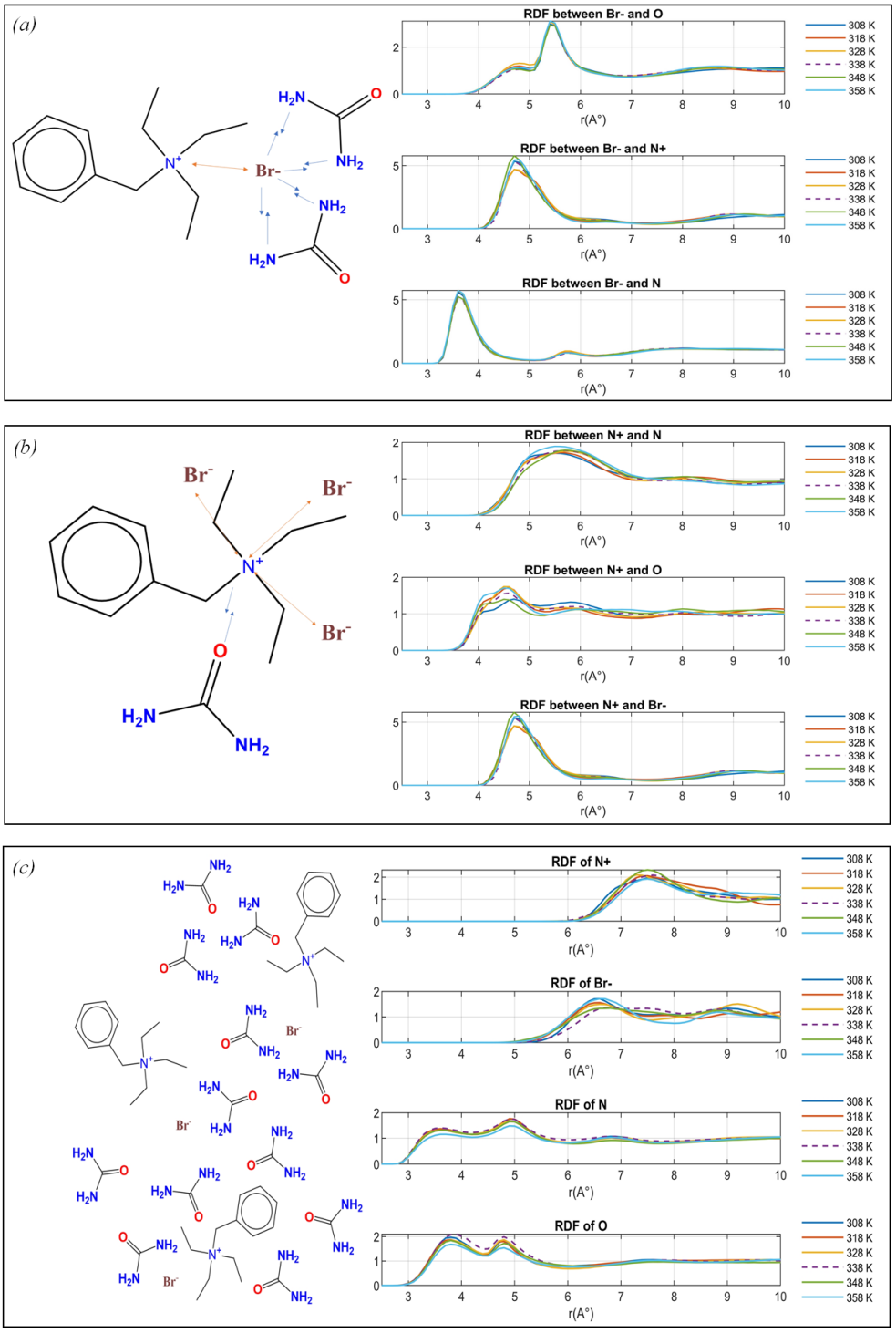

Fig. 5: Radial Distribution Functional (RDF) of atoms (a) around Br- anions (b) around ammonium cation and (c) of atoms system at 308 – 358 K *(Blue double arrow: H-bonds, Orange arrow: Salt bridge)*

The results are important to understand the behavior of DES, where the Br^- charge is compensated by N^+ and amino H-urea, whereas the N^+ charge is recompensed by carbonyl and

Br^- anions. However, the bromide ion and urea (via oxygen atom) compete for the same binding sites on the cation charge center, as well as other urea molecules with urea consistently showing shorter bond distances.[112] In addition, the RDF confirms the formation of two sub-aggregations in bulk N^+: Br^-: urea structure. The temperature affects N^+/Br^- and N^+/O^- RDFs which leads to the weakening of the salt bridge while increasing N^+/O^-electrostatic interactions against increasing temperature. The RDFs of atoms, elucidating the bulk DES structure, are shown in Fig. 5c. RDF results indicate that the ratio of urea molecules in DES and its hydrogen bond acceptor-donor nature weaken the salt bridge interactions between Br^-/N^+, and this is due to the hydrogen bonding of H-urea/Br^- and to electrostatic interactions between O^-urea/N^+, leading to the formation of a stable liquid bulk structure. Moreover, this behavior is favored by the increase in temperature, which plays a central role in the rupture of the network of hydrogen bonds of urea.[113]

Molecular structure of DES-CELL system

MD simulation results in the segregation of cellulose oligomers after 20 ns are shown in Fig. 6. The segregation of chains established is due to the formation of molecular clusters driven by stronger intermolecular interactions (i.e., hydrogen bonds, Pi-Pi stacking, Pi-cation interactions, salt bridge, and hydrophobic stacking), leading to solvation shell formation around cellulose chains.[114] Also, MD results reveal that the strong H-bond interactions of Br^-/OH cellulose groups (Fig. 6bA, 6bB, 6bC, 6bE), urea/OH cellulose groups (Fig. 6bB), and hydrophobic benzyl ring/cellulose ring stacking (Fig. 6bD) competes for the intermolecular hydrogen bond cellulose network, resulting in a stable molecular cluster (Fig. 6c).[115, 116]

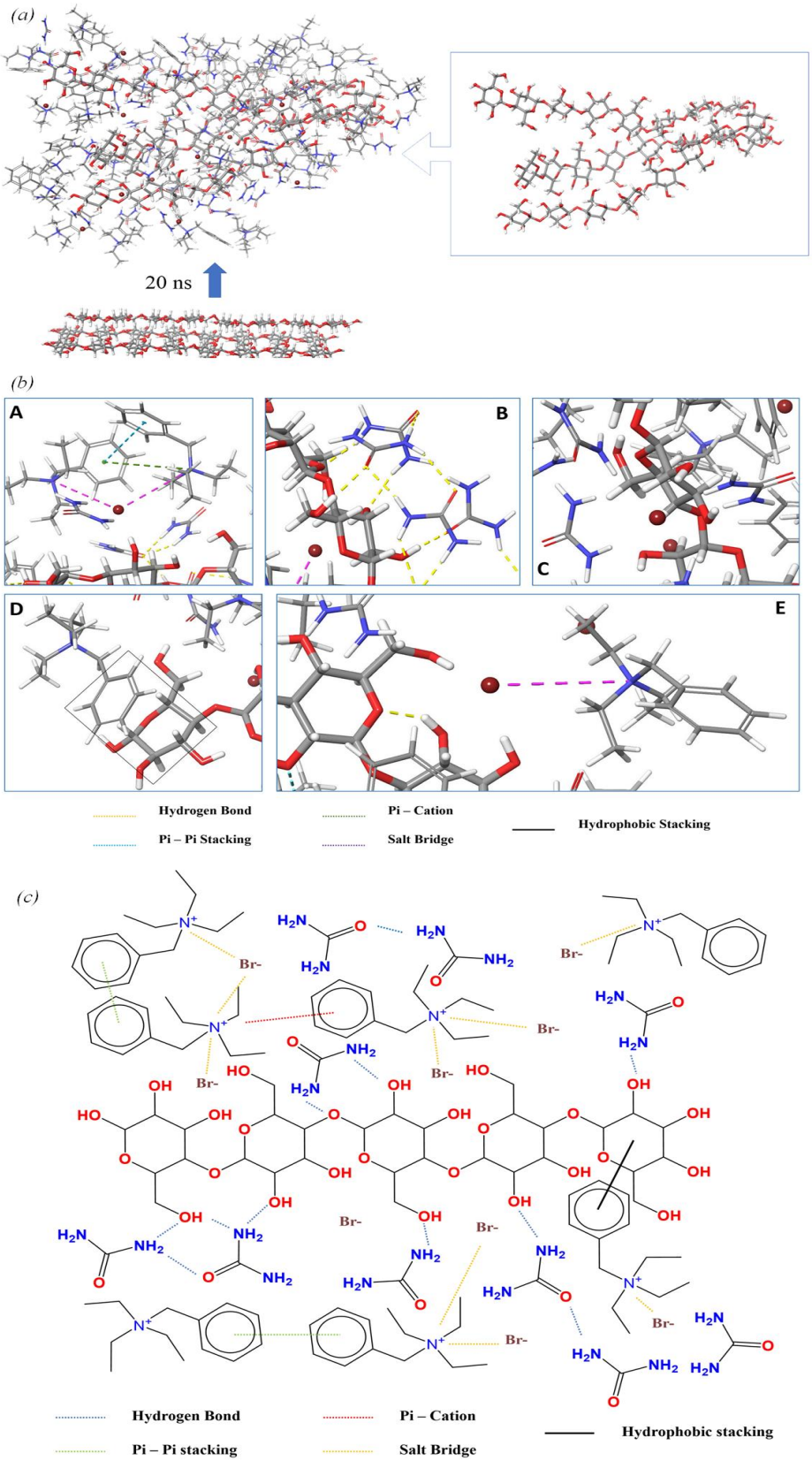

Fig. 6: The cellulose oligomers confirmation (a) after 20 ns MD simulation, (b) with DES after 20 ns MD simulation and (c) Graphic cellulose dissolution mechanism in DES

The MD results reveal the contribution of each DES component in the process of cellulose oligomers disassociation. Fig. 6b reassembles the different DES-CELL sub-clusters, and the urea and cellulose form hydrogen bonds i.e., O-urea/H(OH)-Cell, H-urea/O-Cell (Fig. 6bB), bromide ions and cellulose forms hydrogen bonds i.e., Br^-/ H(OH)-Cell, Br^-/H-urea (Fig. 6bA, 6bC and 6bE). On the other hand, bromide ions also act as a bridge between cellulose and the polar head of Benzyltriethylammonium. The nonpolar nature of both benzylic and cellulose rings leads to the stacking conformation (Fig. 6bE), resulting in the breaking down of intermolecular cellulose H-bond and the solvation shell formation (Fig. 6a and 6c) [116].

3.3. Cellulose dissolution in BTAB/urea DES: Experimental investigation

The limited solubility of various biopolymers, including cellulose, in the majority of solvents, is due to their considerable intra- and inter-molecular H-bonding densities and high molecular weight.[117, 118] Therefore, a suitable solvent system capable of solubilizing cellulose effectively, should possess H-bond rupture properties and exceptionally high ionic strength, where urea is one of the most well-known chemical molecules used to break H-bonds.[119] For this purpose, the ability of novel solvent systems consisting of BTEAB-Urea (1:2) DES to dissolve cellulose has been investigated in this section. Thus, for BTEAB-based DES freshly prepared in a flask placed in an oil bath, under stirred and heated at 60-70° C (*clear and transparent in nature*), desired amounts of cellulose were added, and solubility was estimated in 15 min after each cellulose addition. In case of complete dissolution, approximately 2% more cellulose was continuously added until insoluble solids were observed. Then, time and concentration were recorded against the solubility. Fig. 7 shows that the cellulose solutions in BTEAB-Urea (1: 2) are macroscopically homogeneous although there is a color change for the highest concentrations. As a reminder, the highest concentration of cellulose solubility in a DES containing malic acid and proline is claimed to be 0.78%.[120] In contrast to the relatively high solubility of cellulose in DES described in the literature, such as 6.1wt% in ChCl/Res[121] and 2.48 wt% in ChCl/Im[41], the BTAB/urea DES has shown excellent cellulose solvation properties in the range of 2% to 11% knowing that the results published in the literature generally range from 2 to 6%w.[122] The dissolution results were obtained without any additional pretreatment that might have reduced the degree of crystallinity and DP and no auxiliary component was introduced to the TBEAB-based DESs. Furthermore, cellulose has been shown to be insoluble in choline chloride and ethylene glycol or glycerol-based DESs due to the inability of these

HBD compounds to break H-bonds as in the case of urea-based DESs. We can reasonably assume that the DES compounds containing urea as HBD participate in the formation of H-bonds within the system. The interaction between the solvent system and cellulose, specifically urea, plays a critical role in disrupting the H-bonding network of cellulose and stabilizing the cellulose chains in the medium to form a homogeneous cellulose solution, and consequently, significant solubility of cellulose was achieved.[122] Based on the observations above, BTEAB/urea (1:2) has emerged as the most promising potential 'green' solvent system.

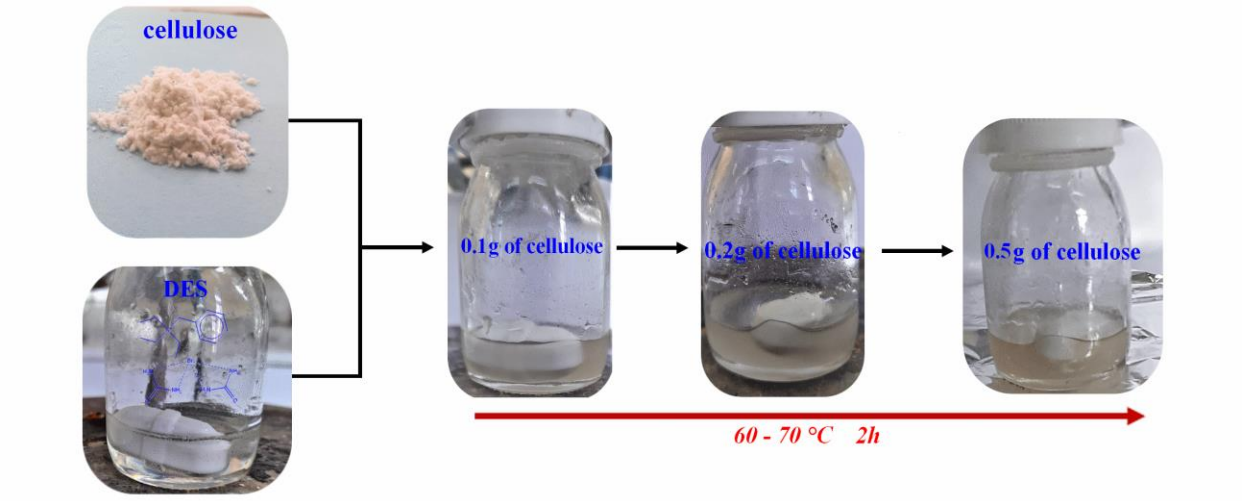

Fig. 7: Macroscopic observations of BTEAB-urea and cellulose/BTEAB-urea mixture with 2.2, 4.4 and 11%w of cellulose at 60-70°C after 2 hours of heating

Experimental viscosity determination is currently one of the most popular and earliest techniques in macromolecular chemistry for the characterization of polymers in solution.[123] The Mark-Houwink-Sakurada (MHS) graphic viscosity method is frequently used to evaluate the average chain length of cellulose and derivatives.[124] Viscosity is directly related to the strength of cohesive forces between molecules, which increase against molecular weight (longer chains) that augments resistance to flow.[125] At this point, the inherent viscosity of the cellulosic solution is directly proportional to the average chain length or viscosity-average molecular weight (Mw) where the corresponding DP is the average degree of polymerization).[126] To determine the structural changes caused by the dissolution of cellulose in DES in particular, the influence of the new solvent on the length of the cellulose chains (the average molecular weight) of the commercial and regenerated cellulose chains was investigated and estimated using the Mark-Houwink equation. Therefore, the intrinsic viscosity [η] was derived from the linear

dependence and extrapolation of reduced and inherent viscosity at zero concentration (Fig. 8). The different viscosities were measured from the flow time of the polymer solution through the glass capillary of the Ubbelohde viscometer, at 25°C in a NaOH/Urea/H_2O solvent according to *El-Barkany et al.* method *(El Idrissi, El Barkany 2013)* and the results are regrouped in Table SD2. In brief, the cellulose samples were dissolved in DES for 4h at 60-70 °C until the complete dissolution of cellulose and the obtaining of transparent clear solutions. Subsequently, the cellulose solutions were cooled to room temperature, and then regenerated from the (cellulose-DES) solution by adding water, filtration under vacuum and then washed frequently and dried at 60 °C overnight and in a desiccator with P_2O_5.

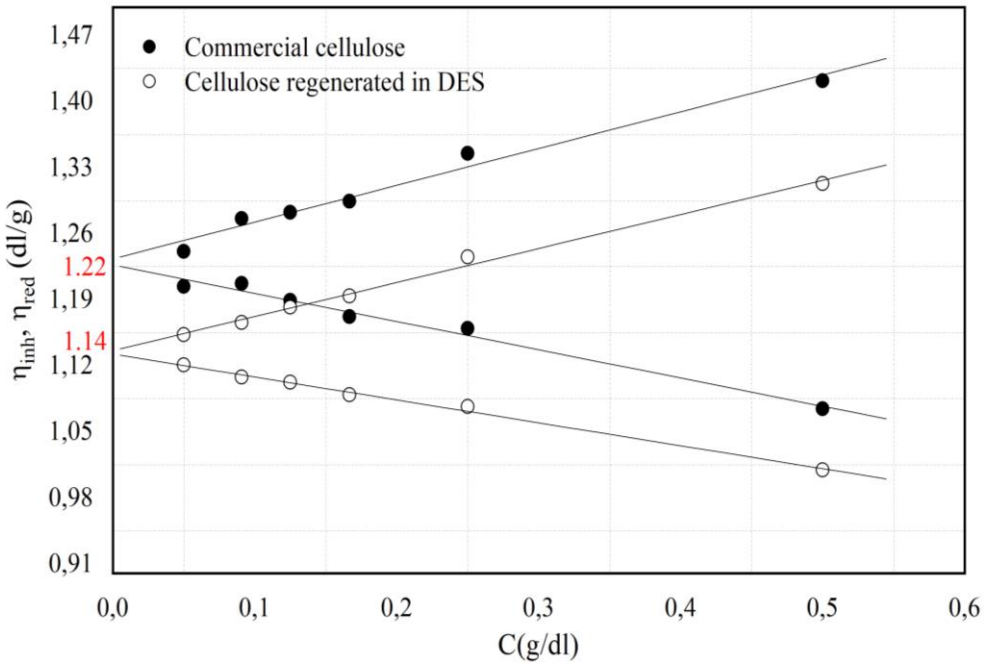

Fig. 8: The intrinsic, inherent and reduced viscosity measurements of commercial and regenerated cellulose

The intrinsic viscosity measurements were performed for a range of concentrations from 0.05 to 0.60 g/dl for the commercial and regenerated cellulose solutions (1g/dl stock solution). The cellulose samples were dissolved in a solution of 6wt% NaOH/4 wt% urea/90wt %H_2O, where the MHS constants were extracted from the work previously reported by *Zhou et al.*[126] In this work, the obtained results show that the average molecular weight of regenerated

cellulose (Mw = 31644 Da, DP = 195) was not affected by the dissolution process in BTEAB/urea DES system compared to that of commercial cellulose (Mw = 34390 Da, DP = 212). The small difference noted is suggested for the structural gain of the amorphous behavior that facilitates penetration of solvent and the mobility of chains.[127] These results are in good agreement with previous studies reported in the literature. Indeed, *Ahn et al*. observed a significant decrease in the average molecular weight of cellulose dissolved in the Bmim[Cl] system.[128] *Rebière* describes the modifications caused by the dissolution of 4 commercial cellulosic samples, with different crystalline rates and degrees of polymerization (DP), in 4 solvent systems,[129] which are known and used to dissolve cellulose and depending on the solvent used to solubilize the samples, some degradation could be observed. In addition, some investigations have revealed a decrease in the value of DP by 50%.[128] However, the cellulose dissolution process in BTEAB/urea was carried out by the rupture of the intra and inter-molecular interactions between the cellulosic chains without length degradation, which made BTEAB/urea affordable as a suitable solvent,[130] where the good solvent for cellulose involves high diffusivity, aggressiveness in decrystallization, and the capability of disassociating the cellulose chains without degradation.[131]

The impact of the cellulose dissolution process in DES (BTEAB/urea) was evaluated by investigating the changes in crystalline behavior and the cellulosic polymorphism of the regenerated cellulose (Fig. 9). The regn-Cell diffractogram displayed the characteristic peaks of cellulose type I polymorphism at Bragg diffraction angle at around 2θ ~15°, 16.5°, 22.7°, and 34.5° attributed to the reticular planes within the Miller (hkl) indices (101), ($10\bar{1}$), (002), and (040), respectively.[132] However, the comparison of the crystallinity indices (C.I.), calculated from the equation (*Eq. 5*) where I_{min} is the minimum intensity between 18° and 19° and I_{max} is the maximal intensity between 22° and 23°,[133] revealed a slight decrease in the crystallinity index (C.I.) after the dissolution (cellulose (87%) and Cel-regen (75%)).

$$\text{C.I.} = 1 - \frac{I_{min}}{I_{max}} \qquad (Eq.\ (5))$$

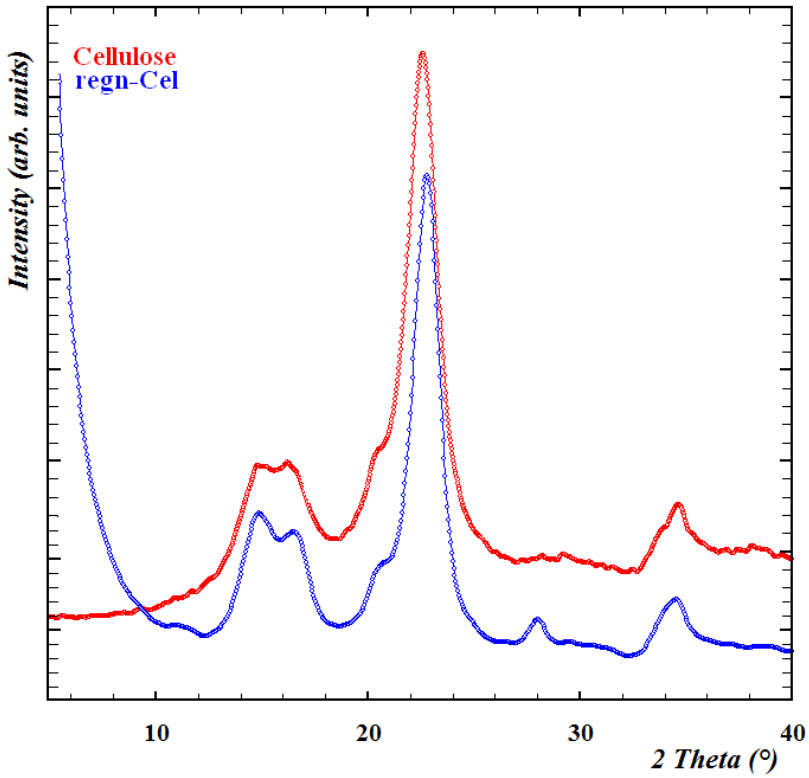

Fig. 9: X-ray diffraction patterns of cellulose and regenerated cellulose (regn-Cell)

In order to improve our knowledge of the nature of DES and to extend their application, detailed insight into their thermodynamic behavior is required. To consider their potential use as solvents, it is extremely important to have insight into the properties of DES mixed with water or organic solvents.[134] The melting point of certain DES is one of the most important limiting factors that inhibit the development of emerging DES-based technologies that could provide promise in various applications. Consequently, one of the most promising possibilities for the development of DES-based processes is the incorporation of a suitable cosolvent.[135] Among the different potential cosolvents, H_2O is preferable because it's both inexpensive and eco-friendly.[136] To better understand the impact of cosolvents on the melting point BTEAB/urea DES system, different quantities of water or DMSO were added to BTEAB/urea DES, and then the eutectic temperatures were measured. The evolution of the eutectic melting point against water or DMSO added quantities (wt. %) was illustrated in Fig. 10.

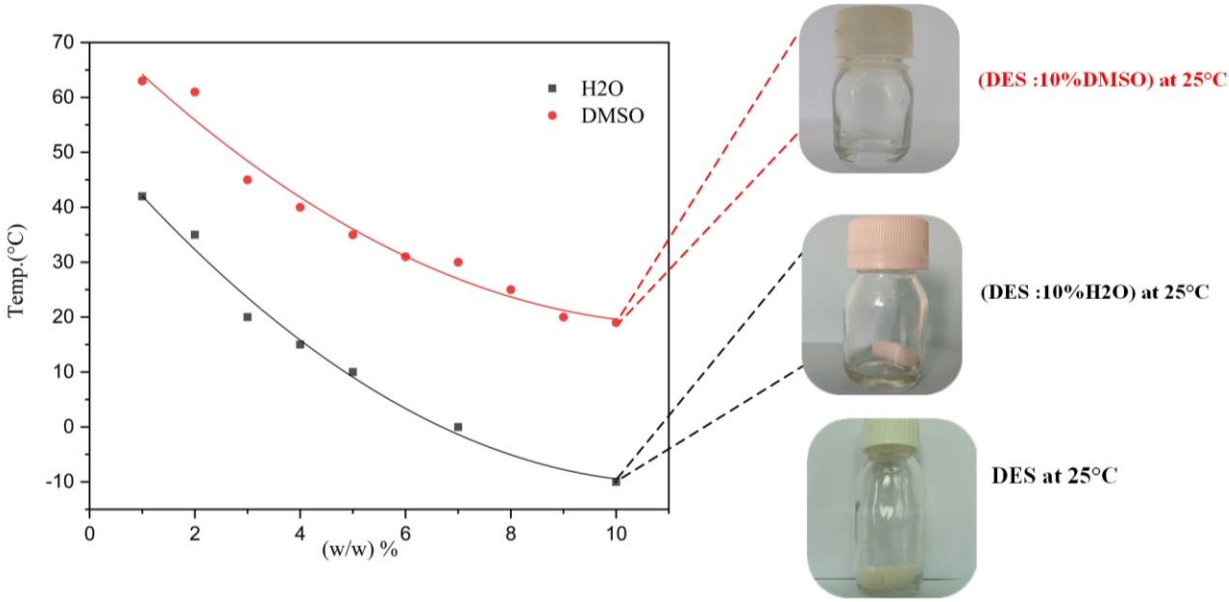

666

667 **Fig. 10**: The evolution of the EMP against water and DMSO added quantities (wt. %)

668 Increasing water or DMSO (cosolvent) added quantities (wt. %), a notable decrease in
669 eutectic melting temperature was observed. As shown in Fig. 10, the melting temperature of the
670 DES-H_2O mixture was drastically decreased from 60-70 °C without water to -15 °C as the H_2O
671 concentration increased to 10 wt. %. However, at the same added quantities (wt. %) of DMSO,
672 the EMP remained around 20°C. comparing the impact of different cosolvents on the properties
673 of DES, it was observed that the addition of water and DMSO could significantly affect the
674 microstructure of DES, resulting in the formation of a new eutectic mixture with a lower melting
675 point than the original DES. This achievement was expected and suggested that H_2O affects the
676 inter-molecular interactions of DES more effectively than DMSO. The difference in the effect
677 can be attributed to the fact that H_2O is protic, which means that it can form an H-bond with
678 other species, such as HBD, allowing the ionization and the solvation of the DES
679 components.[137]

680 The results agree with those reported by *Meng et al.*[138] who examined the effect of water,
681 which can be naturally absorbed by deep eutectic solvents, on the melting point of ChCl:U. The
682 melting point was determined using three different techniques: a thermostated bath, optical
683 microscopy, and Differential Scanning Calorimetry (DSC). The results showed a linear

decrease in melting point with an increase in water content. Specifically, the melting point decreased from 30 °C for the anhydrous deep eutectic solvent to 15 °C in the presence of 5 wt% water. The melting point of 1:1 ChCl: boric acid, on the other hand, was increased slightly by adding up to 10 wt% water, which was explained by a possible water-boric acid reaction.[139] Regarding applications, even 10% H_2O or DMSO content in BTEAB/urea drastically affects its physical properties, especially the melting point. The decrease in the eutectic point of BTEAB/urea DES to around -15°C may hinder the use of DES-H_2O/DMSO as a solvent in organic, electrochemical, and other applications.[140-144]

Conclusion:

In the present work, a new green and eco-friendly DES based on Benzyltriethylammonium bromide was successfully used and studied as a new system for cellulose dissolution and functionalization. As a result, significant solubility of cellulose was obtained; the system emerged as the most promising possible "green" solvent solution, with the ability to dissolve cellulose. Intrinsic viscosity measurements and X-ray diffraction of untreated and regenerated cellulose samples were performed to assess the structural change caused by the dissolution process. The new DES-system has no significant effect on the chain length of the dissolved cellulose samples. However, the comparison of the Crystallinity Indices (C.I.) revealed a slight decrease in the crystallinity of cellulose after dissolution. The results suggest that water has a more significant impact on the inter-molecular interactions of the DES components compared to DMSO. Specifically, adding water to the DES significantly decreased its eutectic point temperature from 60-70 °C to -15 °C, while adding DMSO had a lesser effect, keeping the melting temperature around 20°C. The different solubility properties of cellulose in DES were simulated and computed, and the atomic geometry and electronic properties were calculated using DFT with the B3LYP/6-311+G (d,p) approximation, as well as the H-bond densities and radial distribution functions through molecular dynamics. Both approaches generally provide reasonable results for the interaction and demonstrate that it is the cooperation of each DES component in the process of cellulose disassociation that determines the dissolution efficiency. In summary, the computational data provides insight into the mechanism of cellulose dissolution. A variety of NCIs, including strong and weak hydrogen bonds and electrostatic interactions, play a crucial role in the formation of DES and the dissolving cellulose. The results

from the distribution of EPS, AIM, and RDG suggest that the dissolution of cellulose in BTAB/urea is mainly driven by strong hydrogen bonds. And indicate that the region and the strength of the attractive forces between cellulose and HBD are notably stronger than those between cellulose and HBA, indicating that the urea has a crucial and significant contribution to the cellulose dissolution process. To design an effective DES for cellulose dissolution, an HBD with a small volume, high hydrogen bond basicity, and the ability to form multiple hydrogen bonds is desirable.

Acknowledgments:

We greatly thank the anonymous reviewers for their careful review and valuable suggestions on the manuscript. The authors are thankful to the Head of Oujda's chemistry department and the Head of Physical Measurements, *Prof. Abdelmonaem TALHAOUI*, for providing all the facilities and subsidies necessary to carry out the research work in this article.

References:

1. George, J.; Sabapathi, S., Cellulose nanocrystals: synthesis, functional properties, and applications. *Nanotechnology, science and applications* **2015,** *8*, 45.

2. Shi, Z.; Zhang, Y.; Phillips, G. O.; Yang, G., Utilization of bacterial cellulose in food. *Food hydrocolloids* **2014,** *35*, 539-545.

3. Brinchi, L.; Cotana, F.; Fortunati, E.; Kenny, J., Production of nanocrystalline cellulose from lignocellulosic biomass: technology and applications. *Carbohydrate polymers* **2013,** *94* (1), 154-169.

4. Wang, X.; Yao, C.; Wang, F.; Li, Z., Cellulose-based nanomaterials for energy applications. *Small* **2017,** *13* (42), 1702240.

5. Xu, A.; Wang, Y.; Gao, J.; Wang, J., Facile fabrication of a homogeneous cellulose/polylactic acid composite film with improved biocompatibility, biodegradability and mechanical properties. *Green Chemistry* **2019,** *21* (16), 4449-4456.

6. Jabir, L.; El-Hammi, H.; Mohammed, N.; Jilal, I.; El Idrissi, A.; Amhamdi, H.; Abou-Salama, M.; El Ouardi, Y.; El Barkany, S.; Laatikainen, K., Cellulose based pH-sensitive hydrogel for highly efficient dye removal in water treatment: kinetic, thermodynamic, theoretical and computational studies. *Cellulose* **2022,** *29* (8), 4539-4564.

7. Hallac, B. B.; Ragauskas, A. J., Analyzing cellulose degree of polymerization and its relevancy to cellulosic ethanol. *Biofuels, Bioproducts and Biorefining* **2011,** *5* (2), 215-225.

8. Xia, G.; Wan, J.; Zhang, J.; Zhang, X.; Xu, L.; Wu, J.; He, J.; Zhang, J., Cellulose-based films prepared directly from waste newspapers via an ionic liquid. *Carbohydrate polymers* **2016,** *151*, 223-229.

9. Qi, H., Novel Regenerated Cellulosic Materials. In *Novel Functional Materials Based on Cellulose*, Springer: 2017; pp 25-43.

10. Xu, A.; Wang, J.; Wang, H., Effects of anionic structure and lithium salts addition on the dissolution of cellulose in 1-butyl-3-methylimidazolium-based ionic liquid solvent systems. *Green Chemistry* **2010,** *12* (2), 268-275.

11. Isogai, A.; Hänninen, T.; Fujisawa, S.; Saito, T., Review: Catalytic oxidation of cellulose with nitroxyl radicals under aqueous conditions. *Progress in Polymer Science* **2018,** *86*, 122-148.

12. Wang, S.; Lu, A.; Zhang, L., Recent advances in regenerated cellulose materials. *Progress in Polymer Science* **2016,** *53*, 169-206.

13. Pinkert, A.; Marsh, K. N.; Pang, S.; Staiger, M. P., Ionic liquids and their interaction with cellulose. *Chemical reviews* **2009,** *109* (12), 6712-6728.

14. Sekharan, T. R.; Chandira, R. M.; Tamilvanan, S.; Rajesh, S.; Venkateswarlu, B., Deep eutectic solvents as an alternate to other harmful solvents. *Review* **2022,** *12*, 847-860.

15. Ukai, H.; Inui, S.; Takada, S.; Dendo, J.; Ogawa, J.; Isobe, K.; Ashida, T.; Tamura, M.; Tabuki, K.; Ikeda, M., Types of organic solvents used in small-to medium-scale industries in Japan; a nationwide field survey. *International archives of occupational and environmental health* **1997,** *70* (6), 385-392.

16. Wang, H.; Nie, L.; Li, J.; Wang, Y.; Wang, G.; Wang, J.; Hao, Z., Characterization and assessment of volatile organic compounds (VOCs) emissions from typical industries. *Chinese Science Bulletin* **2013,** *58* (7), 724-730.

17. Kaisar, M. A.; Prasad, S.; Liles, T.; Cucullo, L., A decade of e-cigarettes: limited research & unresolved safety concerns. *Toxicology* **2016,** *365*, 67-75.

18. Baglioni, P.; Baglioni, M.; Bonelli, N.; Chelazzi, D.; Giorgi, R., Smart soft nanomaterials for cleaning. In *Nanotechnologies and nanomaterials for diagnostic, conservation and restoration of cultural heritage*, Elsevier: 2019; pp 171-204.

19. Horváth, I. T., Solvents from nature. *Green Chemistry* **2008,** *10* (10), 1024-1028.

20. Khandelwal, S.; Tailor, Y. K.; Kumar, M., Deep eutectic solvents (DESs) as eco-friendly and sustainable solvent/catalyst systems in organic transformations. *Journal of Molecular Liquids* **2016,** *215*, 345-386.

21. Florindo, C.; Oliveira, F. S.; Rebelo, L. P. N.; Fernandes, A. M.; Marrucho, I. M., Insights into the synthesis and properties of deep eutectic solvents based on cholinium chloride and carboxylic acids. *ACS Sustainable Chemistry & Engineering* **2014,** *2* (10), 2416-2425.

22. Hessel, V.; Tran, N. N.; Asrami, M. R.; Tran, Q. D.; Long, N. V. D.; Escribà-Gelonch, M.; Tejada, J. O.; Linke, S.; Sundmacher, K., Sustainability of green solvents–review and perspective. *Green Chemistry* **2022**.

23. Ahangari, H.; King, J. W.; Ehsani, A.; Yousefi, M., Supercritical fluid extraction of seed oils–A short review of current trends. *Trends in Food Science & Technology* **2021,** *111*, 249-260.

24. Welton, T., Ionic liquids in green chemistry. *Green Chemistry* **2011,** *13* (2), 225-225.

25. Bates, C. M.; Seshimo, T.; Maher, M. J.; Durand, W. J.; Cushen, J. D.; Dean, L. M.; Blachut, G.; Ellison, C. J.; Willson, C. G., Polarity-switching top coats enable orientation of sub–10-nm block copolymer domains. *Science* **2012,** *338* (6108), 775-779.

26. Vanda, H.; Dai, Y.; Wilson, E. G.; Verpoorte, R.; Choi, Y. H., Green solvents from ionic liquids and deep eutectic solvents to natural deep eutectic solvents. *Comptes Rendus Chimie* **2018,** *21* (6), 628-638.

27. Ardila-Fierro, K. J.; Hernández, J. G., Sustainability assessment of mechanochemistry by using the twelve principles of green chemistry. *ChemSusChem* **2021,** *14* (10), 2145-2162.

28. Wu, M.; Bai, Y.; Chen, X.; Wang, Q.; Wang, G., Deep eutectic solvents used as catalysts for synthesis of 1,10-phenanthroline by improved Skraup reaction. *Research on Chemical Intermediates* **2021,** *47* (9), 3551-3567.

29. Tome, L. I.; Baiao, V.; da Silva, W.; Brett, C. M., Deep eutectic solvents for the production and application of new materials. *Applied Materials Today* **2018,** *10*, 30-50.

30. Wang, H.; Liu, S.; Zhao, Y.; Wang, J.; Yu, Z., Insights into the Hydrogen Bond Interactions in Deep Eutectic Solvents Composed of Choline Chloride and Polyols. *ACS Sustainable Chemistry & Engineering* **2019,** *7* (8), 7760-7767.

31. Abbott, A. P.; Capper, G.; Davies, D. L.; Rasheed, R. K.; Tambyrajah, V., Novel solvent properties of choline chloride/urea mixtures. *Chemical Communications* **2003,** (1), 70-71.

32. Tang, B.; Zhang, H.; Row, K. H., Application of deep eutectic solvents in the extraction and separation of target compounds from various samples. *Journal of separation science* **2015,** *38* (6), 1053-1064.

33. Xia, Q.; Liu, Y.; Meng, J.; Cheng, W.; Chen, W.; Liu, S.; Liu, Y.; Li, J.; Yu, H., Multiple hydrogen bond coordination in three-constituent deep eutectic solvents enhances lignin fractionation from biomass. *Green chemistry* **2018,** *20* (12), 2711-2721.

34. Maugeri, Z.; Leitner, W.; de María, P. D., Practical separation of alcohol–ester mixtures using Deep-Eutectic-Solvents. *Tetrahedron Letters* **2012,** *53* (51), 6968-6971.

35. Ogawa, H.; Mori, H., Lithium salt/amide-based deep eutectic electrolytes for lithium-ion batteries: electrochemical, thermal and computational study. *Physical Chemistry Chemical Physics* **2020,** *22* (16), 8853-8863.

816 36. Zhang, Q.; Vigier, K. D. O.; Royer, S.; Jérôme, F., Deep eutectic solvents: syntheses, properties
817 and applications. *Chemical Society Reviews* **2012,** *41* (21), 7108-7146.

818 37. Tang, X.; Zuo, M.; Li, Z.; Liu, H.; Xiong, C.; Zeng, X.; Sun, Y.; Hu, L.; Liu, S.; Lei, T., Green
819 processing of lignocellulosic biomass and its derivatives in deep eutectic solvents. *ChemSusChem* **2017,**
820 *10* (13), 2696-2706.

821 38. Mamilla, J. L.; Novak, U.; Grilc, M.; Likozar, B., Natural deep eutectic solvents (DES) for
822 fractionation of waste lignocellulosic biomass and its cascade conversion to value-added bio-based
823 chemicals. *Biomass and bioenergy* **2019,** *120*, 417-425.

824 39. Škulcová, A.; Kamenská, L.; Kalman, F.; Ház, A.; Jablonský, M.; Čížová, K.; Šurina, I. In *Deep*
825 *eutectic solvents as medium for pretreatment of biomass*, Key Engineering Materials, Trans Tech Publ:
826 2016; pp 17-24.

827 40. Chen, Y.-L.; Zhang, X.; You, T.-T.; Xu, F., Deep eutectic solvents (DESs) for cellulose dissolution:
828 A mini-review. *Cellulose* **2019,** *26* (1), 205-213.

829 41. Ren, H.; Chen, C.; Wang, Q.; Zhao, D.; Guo, S., The properties of choline chloride-based deep
830 eutectic solvents and their performance in the dissolution of cellulose. *BioResources* **2016,** *11* (2),
831 5435-5451.

832 42. Zhang, Q.; Benoit, M.; de Oliveira Vigier, K.; Barrault, J.; Jérôme, F., Green and inexpensive
833 choline-derived solvents for cellulose decrystallization. *Chemistry–A European Journal* **2012,** *18* (4),
834 1043-1046.

835 43. Zhao, Z.; Chen, X.; Ali, M. F.; Abdeltawab, A. A.; Yakout, S. M.; Yu, G., Pretreatment of wheat
836 straw using basic ethanolamine-based deep eutectic solvents for improving enzymatic hydrolysis.
837 *Bioresource technology* **2018,** *263*, 325-333.

838 44. Park, J. H.; Oh, K. W.; Choi, H.-M., Preparation and characterization of cotton fabrics with
839 antibacterial properties treated by crosslinkable benzophenone derivative in choline chloride-based
840 deep eutectic solvents. *Cellulose* **2013,** *20* (4), 2101-2114.

841 45. Abbott, A. P.; Bell, T. J.; Handa, S.; Stoddart, B., O-Acetylation of cellulose and
842 monosaccharides using a zinc based ionic liquid. *Green Chemistry* **2005,** *7* (10), 705-707.

843 46. Supeno, S.; Daik, R.; El-Sheikh, S. M., The synthesis of a macro-initiator from cellulose in a zinc-
844 based ionic liquid. *BioResources* **2014,** *9* (1), 1267-1275.

845 47. Rozas, S.; Benito, C.; Alcalde, R.; Atilhan, M.; Aparicio, S., Insights on the water effect on deep
846 eutectic solvents properties and structuring: The archetypical case of choline chloride + ethylene
847 glycol. *Journal of Molecular Liquids* **2021,** *344*, 117717.

848 48. Malik, A.; Dhattarwal, H. S.; Kashyap, H. K., An Overview of Structure and Dynamics Associated
849 with Hydrophobic Deep Eutectic Solvents and Their Applications in Extraction Processes.
850 *ChemPhysChem* **2022,** *23* (18), e202200239.

851 49. Yadav, N.; Venkatesu, P., Current understanding and insights towards protein stabilization and
852 activation in deep eutectic solvents as sustainable solvent media. *Physical Chemistry Chemical Physics*
853 **2022,** *24* (22), 13474-13509.

854 50. El Idrissi, A.; El Barkany, S.; Amhamdi, H.; Maaroufi, A. K., Physicochemical characterization of
855 celluloses extracted from Esparto "Stipa tenacissima" of Eastern Morocco. *Journal of applied polymer*
856 *science* **2013,** *128* (1), 537-548.

857 51. Azougagh, O.; Essayeh, S.; Achalhi, N.; El Idrissi, A.; Amhamdi, H.; Loutou, M.; El Ouardi, Y.;
858 Salhi, A.; Abou-Salama, M.; El Barkany, S., New benzyltriethylammonium/urea deep eutectic solvent:
859 Quantum calculation and application to hyrdoxylethylcellulose modification. *Carbohydrate Polymers*
860 **2022,** *276*, 118737.

861 52. Singh, R.; Singh, S.; Saxena, D. C., Systematic Evaluation and Studies on the Effect of Octenyl
862 Succinic Anhydride Treatment on Structural, Functional, Morphological, and Flow Properties of
863 Underutilized Chenopodium album Starch. *Starch - Stärke* **2022,** *74* (3-4), 2100217.

864 53. Giraldo, J. D.; Rivas, B. L., Direct ionization and solubility of chitosan in aqueous solutions with
865 acetic acid. *Polymer Bulletin* **2021,** *78* (3), 1465-1488.

866 54. Medronho, B.; Lindman, B., Competing forces during cellulose dissolution: From solvents to
867 mechanisms. *Current Opinion in Colloid & Interface Science* **2014,** *19* (1), 32-40.

868 55. Neto, W. P. F. Morphological investigation of cellulose nanocrystals and nanocomposite
869 applications. Universidade Federal de Uberlândia, 2017.

870 56. Jilal, I.; El-Barkany, S.; Bahari, Z.; Sundman, O.; El-Idrissi, A.; Abou-Salama, M.; Loutou, M.;
871 Ablouh, E.; Amhamdi, H., New benzyloxyethyl cellulose (BEC) crosslinked EDTA: synthesis,
872 characterization and application for supramolecular self-assembling nanoencapsulation of Pb (II).
873 *Materials Today: Proceedings* **2019,** *13*, 909-919.

874 57. Fu, H.; Wang, X.; Sang, H.; Hou, Y.; Chen, X.; Feng, X., Dissolution behavior of microcrystalline
875 cellulose in DBU-based deep eutectic solvents: Insights from spectroscopic investigation and quantum
876 chemical calculations. *Journal of Molecular Liquids* **2020,** *299*, 112140.

877 58. Becke, A. D., A new mixing of Hartree–Fock and local density-functional theories. *The Journal*
878 *of Chemical Physics* **1993,** *98* (2), 1372-1377.

879 59. Lee, C.; Yang, W.; Parr, R. G., Development of the Colle-Salvetti correlation-energy formula
880 into a functional of the electron density. *Physical Review B* **1988,** *37* (2), 785-789.

881 60. Frisch, M.; Trucks, G.; Schlegel, H.; Scuseria, G.; Robb, M.; Cheeseman, J.; Scalmani, G.;
882 Barone, V.; Mennucci, B.; Petersson, G., Gaussian 09, Revision D. 01, Gaussian, Inc., Wallingford CT.
883 *See also: URL: http://www. gaussian. com* **2009**.

884 61. Frisch, A.; Nielson, A.; Holder, A., Gauss view user manual. Pittsburgh, PA: Gaussian. Inc: 2005.

885 62. Bader, R. F. W.; Nguyen-Dang, T. T., Quantum Theory of Atoms in Molecules–Dalton Revisited.
886 In *Advances in Quantum Chemistry*, Löwdin, P.-O., Ed. Academic Press: 1981; Vol. 14, pp 63-124.

887 63. Tognetti, V.; Cortona, P.; Adamo, C., A new parameter-free correlation functional based on an
888 average atomic reduced density gradient analysis. *The Journal of Chemical Physics* **2008,** *128* (3),
889 034101.

890 64. Lu, T.; Chen, F., Multiwfn: A multifunctional wavefunction analyzer. *Journal of Computational*
891 *Chemistry* **2012,** *33* (5), 580-592.

892 65. Humphrey, W.; Dalke, A.; Schulten, K., VMD: Visual molecular dynamics. *Journal of Molecular*
893 *Graphics* **1996,** *14* (1), 33-38.

894 66. Popelier, P.; Aicken, F.; O'Brien, S., Atoms in molecules. *Chemical Modelling: Applications and*
895 *Theory* **2000,** *1*, 143-198.

896 67. Dinda, S.; Samuelson, A. G., The Nature of Bond Critical Points in Dinuclear Copper(I)
897 Complexes. *Chemistry – A European Journal* **2012,** *18* (10), 3032-3042.

898 68. El-Mageed, H. R. A.; Mustafa, F. M.; Abdel-Latif, M. K., Boron nitride nanoclusters,
899 nanoparticles and nanotubes as a drug carrier for isoniazid anti-tuberculosis drug, computational
900 chemistry approaches. *Journal of Biomolecular Structure and Dynamics* **2022,** *40* (1), 226-235.

901 69. Laplaza, R.; Munárriz, J.; Contreras-García, J., Chemical Information. In *Conceptual Density*
902 *Functional Theory*, 2022; pp 349-374.

903 70. Cremer, D.; Kraka, E., A description of the chemical bond in terms of local properties of electron
904 density and energy. *Croatica Chemica Acta* **1984,** *57* (6), 1259-1281.

905 71. Saleh, G.; Gatti, C.; Lo Presti, L.; Contreras-García, J., Revealing non-covalent interactions in
906 molecular crystals through their experimental electron densities. *Chemistry–A European Journal* **2012,**
907 *18* (48), 15523-15536.

908 72. Johnson, E. R.; Keinan, S.; Mori-Sánchez, P.; Contreras-García, J.; Cohen, A. J.; Yang, W.,
909 Revealing Noncovalent Interactions. *Journal of the American Chemical Society* **2010,** *132* (18), 6498-
910 6506.

911 73. Contreras-García, J.; Yang, W.; Johnson, E. R., Analysis of Hydrogen-Bond Interaction
912 Potentials from the Electron Density: Integration of Noncovalent Interaction Regions. *The Journal of*
913 *Physical Chemistry A* **2011,** *115* (45), 12983-12990.

914 74. Dexlin, X. D. D.; Tarika, J. D. D.; Kumar, S. M.; Mariappan, A.; Beaula, T. J., Synthesis and DFT
915 computations on structural, electronic and vibrational spectra, RDG analysis and molecular docking of
916 novel Anti COVID-19 molecule 3, 5 Dimethyl Pyrazolium 3, 5 Dichloro Salicylate. *Journal of Molecular*
917 *Structure* **2021,** *1246*, 131165.

918 75. Jia, Z.; Pang, H.; Li, H.; Wang, X., A density functional theory study on complexation processes
919 and intermolecular interactions of triptycene-derived oxacalixarenes. *Theoretical Chemistry Accounts*
920 **2019,** *138* (9), 113.

921 76. An, X.; Kang, Y.; Li, G., The interaction between chitosan and tannic acid calculated based on
922 the density functional theory. *Chemical Physics* **2019,** *520*, 100-107.

77. Akman, F.; Issaoui, N.; Kazachenko, A. S., Intermolecular hydrogen bond interactions in the thiourea/water complexes (Thio-(H2O)n) (n = 1, …, 5): X-ray, DFT, NBO, AIM, and RDG analyses. *Journal of Molecular Modeling* **2020,** *26* (6), 161.

78. Bowers, K. J.; Chow, E.; Xu, H.; Dror, R. O.; Eastwood, M. P.; Gregersen, B. A.; Klepeis, J. L.; Kolossvary, I.; Moraes, M. A.; Sacerdoti, F. D.; Salmon, J. K.; Shan, Y.; Shaw, D. E., Scalable algorithms for molecular dynamics simulations on commodity clusters. In *Proceedings of the 2006 ACM/IEEE conference on Supercomputing*, Association for Computing Machinery: Tampa, Florida, 2006; pp 84–es.

79. Stalke , D., Meaningful Structural Descriptors from Charge Density. *Chemistry – A European Journal* **2011,** *17* (34), 9264-9278.

80. Panicker, C. Y.; Varghese, H. T.; Manjula, P. S.; Sarojini, B. K.; Narayana, B.; War, J. A.; Srivastava, S. K.; Van Alsenoy, C.; Al-Saadi, A. A., FT-IR, HOMO–LUMO, NBO, MEP analysis and molecular docking study of 3-Methyl-4-{(E)-[4-(methylsulfanyl)-benzylidene]amino}1H-1,2,4-triazole-5(4H)-thione. *Spectrochimica Acta Part A: Molecular and Biomolecular Spectroscopy* **2015,** *151*, 198-207.

81. Özdemir, N.; Eren, B.; Dinçer, M.; Bekdemir, Y., Experimental and ab initio computational studies on 4-(1H-benzo[d]imidazol-2-yl)-N,N-dimethylaniline. *Molecular Physics* **2010,** *108* (1), 13-24.

82. Suryachandram, J.; Prashanth, J.; Bhargavi, D.; Behera, J. N.; Rao, K. P., Investigations of Donor–Acceptor Interactions in 1,3,5-Tris-(3-Methoxy & 3-Methyl Carboxy) Phenyl Ethynyl Benzene Derivatives Using Experimental and DFT Study. *Polycyclic Aromatic Compounds* **2021**, 1-18.

83. Tong, Z.; Meng, J.; Liu, S.; Liu, Y.; Zeng, S.; Wang, L.; Xia, Q.; Yu, H., Room temperature dissolving cellulose with a metal salt hydrate-based deep eutectic solvent. *Carbohydrate Polymers* **2021,** *272*, 118473.

84. Bader, R. F.; Nguyen-Dang, T., Quantum theory of atoms in molecules–Dalton revisited. In *Advances in Quantum Chemistry*, Elsevier: 1981; Vol. 14, pp 63-124.

85. Foroutan-Nejad, C.; Shahbazian, S.; Marek, R., Toward a Consistent Interpretation of the QTAIM: Tortuous Link between Chemical Bonds, Interactions, and Bond/Line Paths. *Chemistry – A European Journal* **2014,** *20* (32), 10140-10152.

86. Chai, K.; Zhou, Y.; Lu, X.; Yamaguchi, T.; Ohara, K.; Liu, H.; Zhu, F., Structure of choline chloride-carboxylic acid deep eutectic solvents by wide-angle X-ray scattering and DFT calculations. *Physical Chemistry Chemical Physics* **2023,** *25* (15), 10481-10494.

87. Desiraju, G. R., A Bond by Any Other Name. *Angewandte Chemie International Edition* **2011,** *50* (1), 52-59.

88. Bondi, A., van der Waals Volumes and Radii. *The Journal of Physical Chemistry* **1964,** *68* (3), 441-451.

89. Mahmoudi, G.; Seth, S. K.; Bauzá, A.; Zubkov, F. I.; Gurbanov, A. V.; White, J.; Stilinović, V.; Doert, T.; Frontera, A., Pb···X (X = N, S, I) tetrel bonding interactions in Pb(ii) complexes: X-ray characterization, Hirshfeld surfaces and DFT calculations. *CrystEngComm* **2018,** *20* (20), 2812-2821.

90. Fuster, F.; Grabowski, S. J., Intramolecular Hydrogen Bonds: the QTAIM and ELF Characteristics. *The Journal of Physical Chemistry A* **2011,** *115* (35), 10078-10086.

91. Espinosa, E.; Alkorta, I.; Elguero, J.; Molins, E., From weak to strong interactions: A comprehensive analysis of the topological and energetic properties of the electron density distribution involving X–H···F–Y systems. *The Journal of Chemical Physics* **2002,** *117* (12), 5529-5542.

92. Pakiari, A. H.; Eskandari, K., The chemical nature of very strong hydrogen bonds in some categories of compounds. *Journal of Molecular Structure: THEOCHEM* **2006,** *759* (1), 51-60.

93. Lande, D. N.; Shewale, M. N.; Gejji, S. P., Host–Guest Interactions Accompanying the Encapsulation of 1,4-Diazabicyclo[2.2.2]octane within endo-Functionalized Macrocycles. *The Journal of Physical Chemistry A* **2017,** *121* (19), 3792-3802.

94. Rozas, I.; Alkorta, I.; Elguero, J., Behavior of Ylides Containing N, O, and C Atoms as Hydrogen Bond Acceptors. *Journal of the American Chemical Society* **2000,** *122* (45), 11154-11161.

95. Cao, B.; Du, J.; Du, D.; Sun, H.; Zhu, X.; Fu, H., Cellobiose as a model system to reveal cellulose dissolution mechanism in acetate-based ionic liquids: Density functional theory study substantiated by NMR spectra. *Carbohydrate Polymers* **2016,** *149*, 348-356.

96. Venkataramanan, N. S.; Suvitha, A.; Kawazoe, Y., Intermolecular interaction in nucleobases and dimethyl sulfoxide/water molecules: A DFT, NBO, AIM and NCI analysis. *Journal of Molecular Graphics and Modelling* **2017,** *78*, 48-60.

97. Koch, U.; Popelier, P. L. A., Characterization of C-H-O Hydrogen Bonds on the Basis of the Charge Density. *The Journal of Physical Chemistry* **1995,** *99* (24), 9747-9754.

98. Li, X.; Li, H.; You, T.; Chen, X.; Ramaswamy, S.; Wu, Y.-Y.; Xu, F., Enhanced Dissolution of Cotton Cellulose in 1-Allyl-3-methylimidazolium Chloride by the Addition of Metal Chlorides. *ACS Sustainable Chemistry & Engineering* **2019,** *7* (23), 19176-19184.

99. Zheng, Y.-Z.; Zhou, Y.; Deng, G.; Guo, R.; Chen, D.-F., The structure and hydrogen-bond behaviours of binary systems containing ionic liquid 1-butyl-3-methylimidazolium tetrafluoroborate and methanol/ethanol. *Spectrochimica Acta Part A: Molecular and Biomolecular Spectroscopy* **2019,** *223*, 117312.

100. Bering, E.; Torstensen, J. Ø.; Lervik, A.; de Wijn, A. S., Computational study of the dissolution of cellulose into single chains: the role of the solvent and agitation. *Cellulose* **2022,** *29* (3), 1365-1380.

101. Sirviö, J. A.; Haataja, R.; Kantola, A. M.; Suopajärvi, T.; Liimatainen, H., Insights into the role of molar ratio and added water in the properties of choline chloride and urea-based eutectic mixtures and their cellulose swelling capacity. *Physical Chemistry Chemical Physics* **2022,** *24* (46), 28609-28620.

102. Alizadeh, V.; Kirchner, B., Molecular level insight into the solvation of cellulose in deep eutectic solvents. *The Journal of Chemical Physics* **2021,** *155* (8), 084501.

103. Saleh , G.; Gatti , C.; Lo Presti, L.; Contreras-García, J., Revealing Non-covalent Interactions in Molecular Crystals through Their Experimental Electron Densities. *Chemistry – A European Journal* **2012,** *18* (48), 15523-15536.

998 104. Firme, C. L.; Monteiro, N. K. V.; Silva, S. R. B., QTAIM and NCI analysis of intermolecular
999 interactions in steroid ligands binding a cytochrome P450 enzyme – Beyond the most obvious
1000 interactions. *Computational and Theoretical Chemistry* **2017,** *1111*, 40-49.

1001 105. Venkataramanan, N. S.; Suvitha, A., Nature of bonding and cooperativity in linear DMSO
1002 clusters: A DFT, AIM and NCI analysis. *Journal of Molecular Graphics and Modelling* **2018,** *81*, 50-59.

1003 106. Zhang, Y.; He, H.; Dong, K.; Fan, M.; Zhang, S., A DFT study on lignin dissolution in imidazolium-
1004 based ionic liquids. *RSC Advances* **2017,** *7* (21), 12670-12681.

1005 107. Wang, J.; Liu, C.; Liu, X.; Shao, L.; Zhang, X.-M., C—H···O hydrogen bonding interactions for
1006 sterically hindered phenols and their phenoxyl radicals. *Journal of Physical Organic Chemistry* **2019,** *32*
1007 (5), e3927.

1008 108. Contreras-García, J.; Johnson, E. R.; Keinan, S.; Chaudret, R.; Piquemal, J.-P.; Beratan, D. N.;
1009 Yang, W., NCIPLOT: A Program for Plotting Noncovalent Interaction Regions. *Journal of Chemical*
1010 *Theory and Computation* **2011,** *7* (3), 625-632.

1011 109. Khalaf, B.; Hamed, O.; Jodeh, S.; Hanbali, G.; Bol, R.; Dagdag, O.; Samhan, S. J. P., Novel,
1012 Environment-Friendly Cellulose-Based Derivatives for Tetraconazole Removal from Aqueous Solution.
1013 **2021,** *13* (3), 450.

1014 110. Hayes, R.; Imberti, S.; Warr, G. G.; Atkin, R., Amphiphilicity determines nanostructure in protic
1015 ionic liquids. *Physical Chemistry Chemical Physics* **2011,** *13* (8), 3237-3247.

1016 111. Chen, Y.; Mu, T., Revisiting greenness of ionic liquids and deep eutectic solvents. *Green*
1017 *Chemical Engineering* **2021**.

1018 112. Brunner, M.; Imberti, S.; Warr, G. G.; Atkin, R., Liquid Structure of Single and Mixed Cation
1019 Alkylammonium Bromide Urea Deep Eutectic Solvents. *The Journal of Physical Chemistry B* **2020,** *124*
1020 (39), 8651-8664.

1021 113. Yadav, A.; Pandey, S., Densities and viscosities of (choline chloride+ urea) deep eutectic solvent
1022 and its aqueous mixtures in the temperature range 293.15 K to 363.15 K. *Journal of Chemical &*
1023 *Engineering Data* **2014,** *59* (7), 2221-2229.

1024 114. Protz, R.; Lehmann, A.; Ganster, J.; Fink, H.-P., Solubility and spinnability of cellulose-lignin
1025 blends in aqueous NMMO. *Carbohydrate Polymers* **2021,** *251*, 117027.

1026 115. Sánchez-Badillo, J. A.; Gallo, M.; Rutiaga-Quiñones, J. G.; López-Albarrán, P., Solvent behavior
1027 of an ionic liquid set around a cellulose Iβ crystallite model through molecular dynamics simulations.
1028 *Cellulose* **2021,** *28* (11), 6767-6795.

1029 116. Manna, B.; Ghosh, A., Dissolution of cellulose in ionic liquid and water mixtures as revealed by
1030 molecular dynamics simulations. *Journal of Biomolecular Structure and Dynamics* **2019,** *37* (15), 3987-
1031 4005.

1032 117. Chen, X.; Zhang, Y.; Wang, H.; Wang, S.-W.; Liang, S.; Colby, R. H., Solution rheology of
1033 cellulose in 1-butyl-3-methyl imidazolium chloride. *Journal of Rheology* **2011,** *55* (3), 485-494.

118. Collier, J. R.; Watson, J. L.; Collier, B. J.; Petrovan, S., Rheology of 1-butyl-3-methylimidazolium chloride cellulose solutions. II. Solution character and preparation. *Journal of Applied Polymer Science* **2009,** *111* (2), 1019-1027.

119. Walters, M. G.; Mando, A. D.; Matthew Reichert, W.; West, C. W.; West, K. N.; Rabideau, B. D., The role of urea in the solubility of cellulose in aqueous quaternary ammonium hydroxide. *RSC Advances* **2020,** *10* (10), 5919-5929.

120. Francisco, M.; van den Bruinhorst, A.; Kroon, M. C., New natural and renewable low transition temperature mixtures (LTTMs): screening as solvents for lignocellulosic biomass processing. *Green Chemistry* **2012,** *14* (8), 2153-2157.

121. Malaeke, H.; Housaindokht, M. R.; Monhemi, H.; Izadyar, M., Deep eutectic solvent as an efficient molecular liquid for lignin solubilization and wood delignification. *Journal of Molecular Liquids* **2018,** *263*, 193-199.

122. Wang, J.; Wang, Y.; Ma, Z.; Yan, L., Dissolution of highly molecular weight cellulose isolated from wheat straw in deep eutectic solvent of Choline/l-Lysine hydrochloride. *Green Energy & Environment* **2020,** *5* (2), 232-239.

123. El Barkany, S.; El Idrissi, A.; Zanagui, C.; Jilal, I.; Tabaght, F.; Abou-Salama, M.; Amhamdi, H., New branched chain cellulose derivatives based on esparto Stipa tenacissima of eastern Morocco: synthesis and characterization. *J Mater Environ Sci* **2017,** *8* (4), 1195-1210.

124. Kumar, R.; Mago, G.; Balan, V.; Wyman, C. E., Physical and chemical characterizations of corn stover and poplar solids resulting from leading pretreatment technologies. *Bioresource Technology* **2009,** *100* (17), 3948-3962.

125. Khayat, K. H.; Mikanovic, N., 8 - Viscosity-enhancing admixtures and the rheology of concrete. In *Understanding the Rheology of Concrete*, Roussel, N., Ed. Woodhead Publishing: 2012; pp 209-228.

126. Zhou, J.; Zhang, L.; Cai, J., Behavior of cellulose in NaOH/Urea aqueous solution characterized by light scattering and viscometry. *Journal of Polymer Science Part B: Polymer Physics* **2004,** *42* (2), 347-353.

127. Gan, S.; Zakaria, S.; Syed Jaafar, S. N., Enhanced mechanical properties of hydrothermal carbamated cellulose nanocomposite film reinforced with graphene oxide. *Carbohydrate Polymers* **2017,** *172*, 284-293.

128. Ahn, Y.; Kwak, S.-Y.; Song, Y.; Kim, H., Physical state of cellulose in BmimCl: dependence of molar mass on viscoelasticity and sol-gel transition. *Physical Chemistry Chemical Physics* **2016,** *18* (3), 1460-1469.

129. Rebière, J.; Heuls, M.; Castignolles, P.; Gaborieau, M.; Rouilly, A.; Violleau, F.; Durrieu, V., Structural modifications of cellulose samples after dissolution into various solvent systems. *Analytical and Bioanalytical Chemistry* **2016,** *408* (29), 8403-8414.

130. Zhu, S.; Wu, Y.; Chen, Q.; Yu, Z.; Wang, C.; Jin, S.; Ding, Y.; Wu, G., Dissolution of cellulose with ionic liquids and its application: a mini-review. *Green Chemistry* **2006,** *8* (4), 325-327.

131. Ghasemi, M.; Tsianou, M.; Alexandridis, P., Assessment of solvents for cellulose dissolution. *Bioresource Technology* **2017,** *228*, 330-338.

132. Perez, S., *Structure et morphologie de la cellulose*. 2000.

133. Nam, S.; French, A. D.; Condon, B. D.; Concha, M., Segal crystallinity index revisited by the simulation of X-ray diffraction patterns of cotton cellulose Iβ and cellulose II. *Carbohydrate Polymers* **2016,** *135*, 1-9.

134. Ma, C.; Laaksonen, A.; Liu, C.; Lu, X.; Ji, X., The peculiar effect of water on ionic liquids and deep eutectic solvents. *Chemical Society Reviews* **2018,** *47* (23), 8685-8720.

135. Shah, D.; Mansurov, U.; Mjalli, F. S., Intermolecular interactions and solvation effects of dimethylsulfoxide on type III deep eutectic solvents. *Physical Chemistry Chemical Physics* **2019,** *21* (31), 17200-17208.

136. Vilková, M.; Płotka-Wasylka, J.; Andruch, V., The role of water in deep eutectic solvent-base extraction. *Journal of Molecular Liquids* **2020,** *304*, 112747.

137. Zainal-Abidin, M. H.; Hayyan, M.; Hayyan, A.; Jayakumar, N. S., New horizons in the extraction of bioactive compounds using deep eutectic solvents: A review. *Analytica Chimica Acta* **2017,** *979*, 1-23.

138. Meng, X.; Ballerat-Busserolles, K.; Husson, P.; Andanson, J.-M., Impact of water on the melting temperature of urea + choline chloride deep eutectic solvent. *New Journal of Chemistry* **2016,** *40* (5), 4492-4499.

139. Häkkinen, R.; Willberg-Keyriläinen, P.; Ropponen, J.; Virtanen, T., Effect of composition and water content on physicochemical properties of choline chloride-boric acid low-melting mixtures. *Journal of Molecular Liquids* **2019,** *280*, 104-110.

140. van Osch, D. J. G. P.; Zubeir, L. F.; van den Bruinhorst, A.; Rocha, M. A. A.; Kroon, M. C., Hydrophobic deep eutectic solvents as water-immiscible extractants. *Green Chemistry* **2015,** *17* (9), 4518-4521.

141. Dhingra, D.; Bhawna; Pandey, A.; Pandey, S., Fluorescence Quenching by Nitro Compounds within a Hydrophobic Deep Eutectic Solvent. *The Journal of Physical Chemistry B* **2020,** *124* (20), 4164-4173.

142. Gera, R.; Moll, C. J.; Bhattacherjee, A.; Bakker, H. J., Water-Induced Restructuring of the Surface of a Deep Eutectic Solvent. *The Journal of Physical Chemistry Letters* **2022,** *13* (2), 634-641.

143. Dai, Y.; Witkamp, G.-J.; Verpoorte, R.; Choi, Y. H., Tailoring properties of natural deep eutectic solvents with water to facilitate their applications. *Food chemistry* **2015,** *187*, 14-19.

144. Harifi-Mood, A. R.; Sadrzadeh, S., Dimethyl sulfoxide/deep eutectic solvents mixtures as media in the reaction of 1-fluoro-2,4-dinitrobenzene with piperidine: A solvent effect study. *Journal of Physical Organic Chemistry* **2018,** *31* (4), e3787.